6-1-2007

Measurement of K^0_S, Λ and Λ̄ Production at HERA

S. Chekanov
Argonne National Laboratory

M. Derrick
Argonne National Laboratory

S. Magill
Argonne National Laboratory

S. Miglioranzi
Argonne National Laboratory

B. Musgrave
Argonne National Laboratory

See next page for additional authors

Eur. Phys. J. C 51, 1–23 (2007)
DOI 10.1140/epjc/s10052-007-0299-2

THE EUROPEAN PHYSICAL JOURNAL C

Regular Article – Experimental Physics

Measurement of K^0_S, Λ and $\bar{\Lambda}$ production at HERA

The ZEUS Collaboration

S. Chekanov[1,a], M. Derrick[1], S. Magill[1], S. Miglioranzi[1,53], B. Musgrave[1], D. Nicholass[1,53], J. Repond[1], R. Yoshida[1], M.C.K. Mattingly[2], M. Jechow[3], N. Pavel[3,b], A.G. Yagües Molina[3], S. Antonelli[4], P. Antonioli[4], G. Bari[4], M. Basile[4], L. Bellagamba[4], M. Bindi[4], D. Boscherini[4], A. Bruni[4], G. Bruni[4], L. Cifarelli[4], F. Cindolo[4], A. Contin[4], M. Corradi[4,54], S. De Pasquale[4], G. Iacobucci[4], A. Margotti[4], R. Nania[4], A. Polini[4], L. Rinaldi[4], G. Sartorelli[4], A. Zichichi[4], D. Bartsch[5], I. Brock[5], S. Goers[5,c], H. Hartmann[5], E. Hilger[5], H.-P. Jakob[5], M. Jüngst[5], O.M. Kind[5], E. Paul[5,d], J. Rautenberg[5,55], R. Renner[5], U. Samson[5], V. Schönberg[5], R. Shehzadi[5], M. Wang[5,56], M. Wlasenko[5], N.H. Brook[6], G.P. Heath[6], J.D. Morris[6], T. Namsoo[6], M. Capua[7], S. Fazio[7], A. Mastroberardino[7], M. Schioppa[7], G. Susinno[7], E. Tassi[7], J.Y. Kim[8,e], K.J. Ma[8,f], Z.A. Ibrahim[9], B. Kamaluddin[9], W.A.T. Wan Abdullah[9], Y. Ning[10], Z. Ren[10], F. Sciulli[10], J. Chwastowski[11], A. Eskreys[11], J. Figiel[11], A. Galas[11], M. Gil[11], K. Olkiewicz[11], P. Stopa[11], L. Zawiejski[11], L. Adamczyk[12], T. Bołd[12], I. Grabowska-Bołd[12], D. Kisielewska[12], J. Łukasik[12], M. Przybycień[12], L. Suszycki[12], A. Kotański[13,g], W. Słomiński[13], V. Adler[14], U. Behrens[14], I. Bloch[14], A. Bonato[14], K. Borras[14], N. Coppola[14], J. Fourletova[14], A. Geiser[14], D. Gladkov[14], P. Göttlicher[14,57], I. Gregor[14], T. Haas[14], W. Hain[14], C. Horn[14], B. Kahle[14], U. Kötz[14], H. Kowalski[14], E. Lobodzinska[14], B. Löhr[14], R. Mankel[14], I.-A. Melzer-Pellmann[14], A. Montanari[14], D. Notz[14], A.E. Nuncio-Quiroz[14], R. Santamarta[14], U. Schneekloth[14], A. Spiridonov[14,58], H. Stadie[14], U. Stösslein[14], D. Szuba[14,59], J. Szuba[14,60], T. Theedt[14], G. Wolf[14], K. Wrona[14], C. Youngman[14], W. Zeuner[14], W. Lohmann[15], S. Schlenstedt[15], G. Barbagli[16], E. Gallo[16,h], P.G. Pelfer[16], A. Bamberger[17], D. Dobur[17], F. Karstens[17], N.N. Vlasov[17,i], P.J. Bussey[18], A.T. Doyle[18], W. Dunne[18], J. Ferrando[18], D.H. Saxon[18], I.O. Skillicorn[18], I. Gialas[19,j], T. Gosau[20], U. Holm[20], R. Klanner[20], E. Lohrmann[20], H. Salehi[20], P. Schleper[20], T. Schörner-Sadenius[20], J. Sztuk[20], K. Wichmann[20], K. Wick[20], C. Foudas[21], C. Fry[21], K.R. Long[21], A.D. Tapper[21], M. Kataoka[22,61], T. Matsumoto[22], K. Nagano[22], K. Tokushuku[22,62], S. Yamada[22], Y. Yamazaki[22], A.N. Barakbaev[23], E.G. Boos[23], A. Dossanov[23], N.S. Pokrovskiy[23], B.O. Zhautykov[23], D. Son[24], J. de Favereau[25], K. Piotrzkowski[25], F. Barreiro[26], C. Glasman[26,k], M. Jimenez[26], L. Labarga[26], J. del Peso[26], E. Ron[26], M. Soares[26], J. Terrón[26], M. Zambrana[26], F. Corriveau[27], C. Liu[27], R. Walsh[27], C. Zhou[27], T. Tsurugai[28], A. Antonov[29], B.A. Dolgoshein[29], I. Rubinsky[29], V. Sosnovtsev[29], A. Stifutkin[29], S. Suchkov[29], R.K. Dementiev[30], P.F. Ermolov[30], L.K. Gladilin[30], I.I. Katkov[30], L.A. Khein[30], I.A. Korzhavina[30], V.A. Kuzmin[30], B.B. Levchenko[30,l], O.Y. Lukina[30], A.S. Proskuryakov[30], L.M. Shcheglova[30], D.S. Zotkin[30], S.A. Zotkin[30], I. Abt[31], C. Büttner[31], A. Caldwell[31], D. Kollar[31], W.B. Schmidke[31], J. Sutiak[31], G. Grigorescu[32], A. Keramidas[32], E. Koffeman[32], P. Kooijman[32], A. Pellegrino[32], H. Tiecke[32], M. Vázquez[32,61], L. Wiggers[32], N. Brümmer[33], B. Bylsma[33], L.S. Durkin[33], A. Lee[33], T.Y. Ling[33], P.D. Allfrey[34], M.A. Bell[34], A.M. Cooper-Sarkar[34], A. Cottrell[34], R.C.E. Devenish[34], B. Foster[34], K. Korcsak-Gorzo[34], S. Patel[34], V. Roberfroid[34,m], A. Robertson[34], P.B. Straub[34], C. Uribe-Estrada[34], R. Walczak[34], P. Bellan[35], A. Bertolin[35], R. Brugnera[35], R. Carlin[35], R. Ciesielski[35], F. Dal Corso[35], S. Dusini[35], A. Garfagnini[35], S. Limentani[35], A. Longhin[35], L. Stanco[35], M. Turcato[35], B.Y. Oh[36], A. Raval[36], J. Ukleja[36,n], J.J. Whitmore[36,o], Y. Iga[37], G. D'Agostini[38], G. Marini[38], A. Nigro[38], J.E. Cole[39], J.C. Hart[39], H. Abramowicz[40,63], A. Gabareen[40], R. Ingbir[40], S. Kananov[40], A. Levy[40], M. Kuze[41], R. Hori[42], S. Kagawa[42,64], N. Okazaki[42], S. Shimizu[42], T. Tawara[42], R. Hamatsu[43], H. Kaji[43,65], S. Kitamura[43,p], O. Ota[43], Y.D. Ri[43], M.I. Ferrero[44], V. Monaco[44], R. Sacchi[44], A. Solano[44], M. Arneodo[45], M. Ruspa[45], S. Fourletov[46], J.F. Martin[46], S.K. Boutle[47,i], J.M. Butterworth[47], C. Gwenlan[47,q], T.W. Jones[47], J.H. Loizides[47], M.R. Sutton[47,o], C. Targett-Adams[47], M. Wing[47], B. Brzozowska[48], J. Ciborowski[48,66], G. Grzelak[48], P. Kulinski[48], P. Łużniak[48,67], J. Malka[48,67], R.J. Nowak[48], J.M. Pawlak[48], T. Tymieniecka[48], A. Ukleja[48,r], A.F. Żarnecki[48], M. Adamus[49], P. Plucinski[49,s], Y. Eisenberg[50], I. Giller[50], D. Hochman[50], U. Karshon[50], M. Rosin[50], E. Brownson[51], T. Danielson[51], A. Everett[51], D. Kçira[51], D.D. Reeder[51], P. Ryan[51], A.A. Savin[51], W.H. Smith[51], H. Wolfe[51], S. Bhadra[52], C.D. Catterall[52], Y. Cui[52], G. Hartner[52], S. Menary[52], U. Noor[52], J. Standage[52], J. Whyte[52]

[1] Argonne National Laboratory, Argonne, Illinois 60439-4815, USA[t]
[2] Andrews University, Berrien Springs, Michigan 49104-0380, USA
[3] Institut für Physik der Humboldt-Universität zu Berlin, Berlin, Germany
[4] University and INFN Bologna, Bologna, Italy[u]
[5] Physikalisches Institut der Universität Bonn, Bonn, Germany[v]
[6] H.H. Wills Physics Laboratory, University of Bristol, Bristol, UK[w]
[7] Calabria University, Physics Department and INFN, Cosenza, Italy[s]
[8] Chonnam National University, Kwangju, South Korea[x]

[9] Jabatan Fizik, Universiti Malaya, 50603 Kuala Lumpur, Malaysia[y]
[10] Nevis Laboratories, Columbia University, Irvington on Hudson, New York 10027, USA[z]
[11] The Henryk Niewodniczanski Institute of Nuclear Physics, Polish Academy of Sciences, Cracow, Poland[aa]
[12] Faculty of Physics and Applied Computer Science, AGH-University of Science and Technology, Cracow, Poland[ab]
[13] Department of Physics, Jagellonian University, Cracow, Poland
[14] Deutsches Elektronen-Synchrotron DESY, Hamburg, Germany
[15] Deutsches Elektronen-Synchrotron DESY, Zeuthen, Germany
[16] University and INFN, Florence, Italy[s]
[17] Fakultät für Physik der Universität Freiburg i.Br., Freiburg i.Br., Germany[t]
[18] Department of Physics and Astronomy, University of Glasgow, Glasgow, UK[u]
[19] Department of Engineering in Management and Finance, University of Aegean, Mytilene, Greece
[20] Hamburg University, Institute of Exp. Physics, Hamburg, Germany[t]
[21] Imperial College London, High Energy Nuclear Physics Group, London, UK[u]
[22] Institute of Particle and Nuclear Studies, KEK, Tsukuba, Japan[ac]
[23] Institute of Physics and Technology of Ministry of Education and Science of Kazakhstan, Almaty, Kazakhstan
[24] Kyungpook National University, Center for High Energy Physics, Daegu, South Korea[v]
[25] Institut de Physique Nucléaire, Université Catholique de Louvain, Louvain-la-Neuve, Belgium[ad]
[26] Departamento de Física Teórica, Universidad Autónoma de Madrid, Madrid, Spain[ae]
[27] Department of Physics, McGill University, Montréal, Québec, H3A 2T8 Canada[af]
[28] Meiji Gakuin University, Faculty of General Education, Yokohama, Japan[aa]
[29] Moscow Engineering Physics Institute, Moscow, Russia[ag]
[30] Moscow State University, Institute of Nuclear Physics, Moscow, Russia[ah]
[31] Max-Planck-Institut für Physik, München, Germany
[32] NIKHEF and University of Amsterdam, Amsterdam, Netherlands[ai]
[33] Physics Department, Ohio State University, Columbus, Ohio 43210, USA[n]
[34] Department of Physics, University of Oxford, Oxford, UK[u]
[35] Dipartimento di Fisica dell' Università and INFN, Padova, Italy[s]
[36] Department of Physics, Pennsylvania State University, University Park, Pennsylvania 16802, USA[x]
[37] Polytechnic University, Sagamihara, Japan[aa]
[38] Dipartimento di Fisica, Università 'La Sapienza' and INFN, Rome, Italy[s]
[39] Rutherford Appleton Laboratory, Chilton, Didcot, Oxon, UK[u]
[40] Raymond and Beverly Sackler Faculty of Exact Sciences, School of Physics, Tel-Aviv University, Tel-Aviv, Israel[aj]
[41] Department of Physics, Tokyo Institute of Technology, Tokyo, Japan[aa]
[42] Department of Physics, University of Tokyo, Tokyo, Japan[aa]
[43] Tokyo Metropolitan University, Department of Physics, Tokyo, Japan[aa]
[44] Università di Torino and INFN, Torino, Italy[s]
[45] Università del Piemonte Orientale, Novara, and INFN, Torino, Italy[s]
[46] Department of Physics, University of Toronto, Toronto, Ontario, M5S 1A7, Canada[ad]
[47] Physics and Astronomy Department, University College London, London, UK[u]
[48] Warsaw University, Institute of Experimental Physics, Warsaw, Poland
[49] Institute for Nuclear Studies, Warsaw, Poland
[50] Department of Particle Physics, Weizmann Institute, Rehovot, Israel[ak]
[51] Department of Physics, University of Wisconsin, Madison, Wisconsin 53706, USA[r]
[52] Department of Physics, York University, Ontario, M3J 1P3, Canada[ad]
[53] also affiliated with University College London, London, UK
[54] also at University of Hamburg, Germany, Alexander von Humboldt Fellow, Hamburg
[55] now at Univ. of Wuppertal, Wuppertal, Germany
[56] now at University of Regina, Regina, Canada
[57] now at DESY group FEB, Hamburg, Germany
[58] also at Institut of Theoretical and Experimental Physics, Moscow, Russia
[59] also at INP, Cracow, Poland
[60] on leave of absence from FPACS, AGH-UST, Cracow, Poland
[61] now at CERN, Geneva, Switzerland
[62] also at University of Tokyo, Tokyo, Japan
[63] also at Max Planck Institute, Munich, Germany, Alexander von Humboldt Research Award
[64] now at KEK, Tsukuba, Japan
[65] now at Nagoya University, Nagoya, Japan
[66] also at Łódź University, Łódź, Poland
[67] Łódź University, Łódź, Poland

Received: 12 December 2006 / Revised version: 19 March 2007 /
Published online: 28 April 2007 –

Abstract. The production of the neutral strange hadrons K^0_S, Λ and $\bar{\Lambda}$ has been measured in ep collisions at HERA using the ZEUS detector. Cross sections, baryon-to-meson ratios, relative yields of strange and charged light hadrons, Λ ($\bar{\Lambda}$) asymmetry and polarization have been measured in three kinematic regions: $Q^2 > 25\,\mathrm{GeV}^2$; $5 < Q^2 < 25\,\mathrm{GeV}^2$; and in photoproduction ($Q^2 \simeq 0$). In photoproduction the presence of two hadronic jets, each with at least 5 GeV transverse energy, was required. The measurements agree in general with Monte Carlo models and are consistent with measurements made at e^+e^- colliders, except for an enhancement of baryon relative to meson production in photoproduction.

[a] Supported by DESY, Germany.
[b] Deceased.
[c] Self-employed.
[d] Retired.
[e] Supported by Chonnam National University in 2005.
[f] Supported by a scholarship of the World Laboratory Björn Wiik Research Project.
[g] Supported by the research grant no. 1 P03B 04529 (2005–2008).
[h] e-mail: gallo@mail.desy.de
[i] Partly supported by Moscow State University, Russia.
[j] Also affiliated with DESY.
[k] Ramón y Cajal Fellow
[l] Partly supported by Russian Foundation for Basic.
[m] EU Marie Curie Fellow
[n] Partially supported by Warsaw University, Poland.
[o] This material was based on work supported by the National Science Foundation, while working at the Foundation.
[p] Department of Radiological Science
[q] PPARC Advanced fellow
[r] Supported by the Polish Ministry for Education and Science grant no. 1 P03B 12629.
[s] Supported by the Polish Ministry for Education and Science grant no. 1 P03B 14129.
[t] Supported by the US Department of Energy.
[u] Supported by the Italian National Institute for Nuclear Physics (INFN).
[v] Supported by the German Federal Ministry for Education and Research (BMBF), under contract numbers HZ1GUA 2, HZ1GUB 0, HZ1PDA 5, HZ1VFA 5.
[w] Supported by the Particle Physics and Astronomy Research Council, UK.
[x] Supported by the Korean Ministry of Education and Korea Science and Engineering Foundation.
[y] Supported by the Malaysian Ministry of Science, Technology and Innovation/Akademi Sains Malaysia grant SAGA 66-02-03-0048.
[z] Supported by the US National Science Foundation. Any opinion, findings and conclusions or recommendations expressed in this material are those of the authors and do not necessarily reflect the views of the National Science Foundation.
[aa] Supported by the Polish State Committee for Scientific Research, grant no. 620/E-77/SPB/DESY/P-03/DZ 117/2003-2005 and grant no. 1P03B07427/2004-2006.
[ab] Supported by the Polish Ministry of Science and Higher Education.
[ac] Supported by the Japanese Ministry of Education, Culture, Sports, Science and Technology (MEXT) and its grants for Scientific Research.
[ad] Supported by FNRS and its associated funds (IISN and FRIA) and by an Inter-University Attraction Poles Programme subsidised by the Belgian Federal Science Policy Office.

1 Introduction

Production of K^0_S, Λ and $\bar{\Lambda}$ hadrons has been extensively studied at particle colliders: e^+e^- [1–15], ep [16–19], $p\bar{p}$ [20–23] and pp [24]. The data have been used to test QCD and build phenomenological models extending QCD predictions beyond what can be calculated from first principles.

The results on K^0_S, Λ, and $\bar{\Lambda}$ production presented in this paper are based on a data sample of 121 pb^{-1} collected by the ZEUS experiment at HERA, about 100 times larger than used in previous HERA publications [16–19] and extend the kinematical region of the measurements, thereby providing a tighter constraint on models.

The measurements have been performed in three different regions of Q^2, where Q^2 is the virtuality of the exchanged boson: deep inelastic scattering (DIS) with $Q^2 > 25\,\mathrm{GeV}^2$; DIS with $5 < Q^2 < 25\,\mathrm{GeV}^2$; and photoproduction, $Q^2 \simeq 0\,\mathrm{GeV}^2$, in which a quasi-real photon interacts with the proton. In the photoproduction sample, two jets, each of at least 5 GeV transverse energy, were required.

The following measurements are presented in this paper: differential cross sections, baryon–antibaryon asymmetry, baryon-to-meson ratio, ratio of strange-to-light hadrons, and the Λ and $\bar{\Lambda}$ transverse spin polarization. There was no attempt to separate direct production from resonance decays: all sources for K^0_S, Λ, and $\bar{\Lambda}$ production were included. These measurements are relevant for modeling production of hadrons at high energies, for example in Monte Carlo (MC) programs [25–29], and for testing the mechanism for baryon transport along the rapidity axis [30], the mechanisms for baryon production [31, 32],

[ae] Supported by the Spanish Ministry of Education and Science through funds provided by CICYT.
[af] Supported by the Natural Sciences and Engineering Research Council of Canada (NSERC).
[ag] Partially supported by the German Federal Ministry for Education and Research (BMBF).
[ah] Supported by RF Presidential grant N 1685.2003.2 for the leading scientific schools and by the Russian Ministry of Education and Science through its grant for Scientific Research on High Energy Physics.
[ai] Supported by the Netherlands Foundation for Research on Matter (FOM).
[aj] Supported by the German-Israeli Foundation and the Israel Science Foundation.
[ak] Supported in part by the MINERVA Gesellschaft für Forschung GmbH, the Israel Science Foundation (grant no. 293/02-11.2) and the U.S.-Israel Binational Science Foundation.

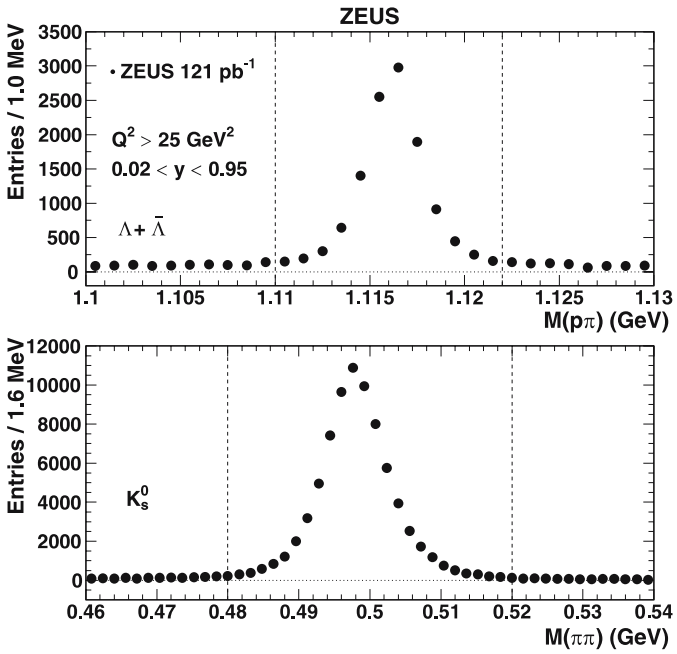

Fig. 1. Mass distributions of the secondary vertex candidates in the $\Lambda+\bar{\Lambda}$ and K^0_S samples assuming $p\pi$ and $\pi\pi$ decays respectively. Only candidates in the range $0.6 < P_{\rm T}^{\rm LAB} < 2.5$ GeV and $|\eta^{\rm LAB}| < 1.2$ for events with $Q^2 > 25$ GeV^2 and $0.02 < y < 0.95$ are displayed. Statistical errors are smaller than the point size. The number of total $\Lambda+\bar{\Lambda}$ and K^0_S candidates located within the *vertical lines* are estimated to be 10 731 and 73 140, respectively, after the background subtraction

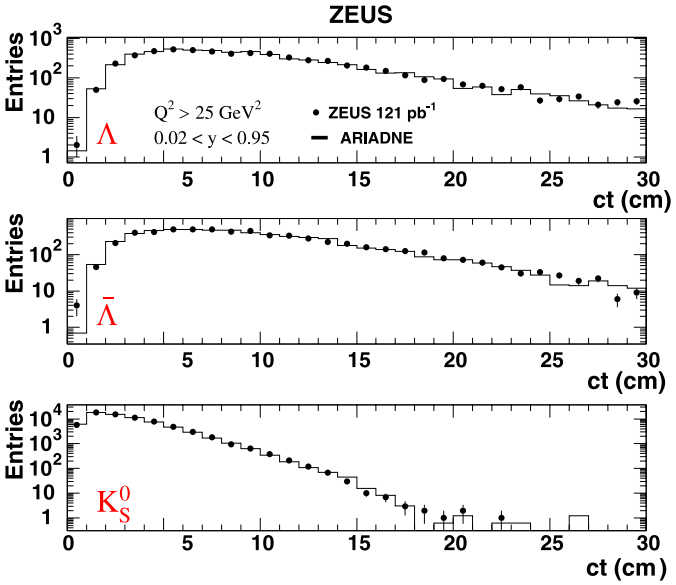

Fig. 2. Detector-level distributions of ct, where t is the reconstructed proper lifetime, for Λ, $\bar{\Lambda}$ and K^0_S samples for data and ARIADNE. The ARIADNE histogram is normalised to the same number of events as the data. Statistical errors are shown unless smaller than the point size

effects due to QCD instantons [33–43] and the mechanisms for the transverse spin polarization of hadrons [44–46].

2 Experimental setup

The data were collected by the ZEUS detector at the HERA ep collider during the running period 1996–2000. The data correspond to an integrated luminosity of 121 pb^{-1}, of which 82 pb^{-1} were collected at $\sqrt{s} = 318$ GeV (the electron or positron beam[1] energy, $E_{\rm e}^{\rm beam}$, was 27.5 GeV and the proton beam energy was 920 GeV) and 39 pb^{-1} at $\sqrt{s} = 300$ GeV (where the proton beam energy was 820 GeV).

A detailed description of the ZEUS detector can be found elsewhere [47]. A brief outline of the components that are most relevant for this analysis is given below.

Charged particles are tracked in the central tracking detector (CTD) [48–50], which operates in a magnetic field of 1.43 Tesla provided by a thin superconducting coil. The CTD consists of 72 cylindrical drift chamber layers, organized in 9 superlayers covering the polar-angle[2] region $15° < \theta < 164°$. The transverse-momentum resolution for full-length tracks is $\sigma(p_{\rm T})/p_{\rm T} = 0.0058 p_{\rm T} \oplus 0.0065 \oplus 0.0014/p_{\rm T}$, with $p_{\rm T}$ in GeV.

The high-resolution uranium-scintillator calorimeter (CAL) [51–54] consists of three parts: the forward (FCAL), the barrel (BCAL) and the rear (RCAL) calorimeters. Each part is subdivided transversely into towers and longitudinally into one electromagnetic section and either one (in RCAL) or two (in BCAL and FCAL) hadronic sections. The smallest subdivision of the calorimeter is called a cell. The CAL energy resolutions, as measured under test-beam conditions, are $\sigma(E)/E = 0.18/\sqrt{E}$ for electrons and $\sigma(E)/E = 0.35/\sqrt{E}$ for hadrons, with E in GeV.

A three-level trigger system was used to select events on-line [47]. At the third level, DIS events were accepted on the basis of the identification of a scattered electron candidate using localised energy deposition in the CAL. As there was no possibility to select inclusive photoproduction sample, the requirement for photoproduction events [55] was based on running a jet algorithm using the energies and positions of the CAL cells. Events with at least two jets were accepted, where each jet was required to have transverse energy greater than 4.5 GeV and pseudorapidity[3] less than 2.5.

The luminosity was measured using the bremsstrahlung process $ep \to ep\gamma$ with the luminosity monitor [56–58], a lead-scintillator calorimeter placed in the HERA tunnel at $Z = -107$ m.

[1] In the text, electron beam, as well as scattered electron, apply to both electron and positron.

[2] The ZEUS coordinate system is a right-handed Cartesian system, with the Z axis pointing in the proton beam direction, referred to as the "forward direction", and the X axis pointing left towards the center of HERA. The coordinate origin is at the nominal interaction point.

[3] The pseudorapidity η is defined as $\eta \equiv -\ln\tan(\theta/2)$, where θ is a scattering angle.

3 Event reconstruction and selection

3.1 Deep inelastic scattering sample

The DIS events are characterised by a scattered electron detected in the CAL. The scattered electron was identified from the energy deposit in the CAL using a neural network [59, 60]. The Bjorken variable $x_{\rm Bj}$ [61] and Q^2 were reconstructed using the double angle method (DA) [62, 63] which has the best resolution in the Q^2 region studied. The inelasticity variable, y, was reconstructed using both the electron (e) [62, 63] and Jacquet–Blondel (JB) [64] methods. The following requirements were applied offline to select events with $Q^2 > 25$ GeV^2 (called the high-Q^2 sample):

- $|\, Z_{\rm vtx}\,| < 50$ cm to reduce the background from non-ep collisions;
- $38 < \delta < 65$ GeV, where $\delta = \sum_i (E_i - P_{Z,i})$ and the sum runs over the energy and longitudinal momentum of all CAL cell deposits. This cut reduced the background from photoproduction and events with large radiative corrections;
- an identified scattered electron with energy above 10 GeV;
- the impact position of the scattered electron on the CAL satisfied $\sqrt{X^2+Y^2} > 36$ cm;
- the electron was isolated: the energy from all CAL cell deposits not associated with the scattered electron but in an $\eta - \phi$ cone of radius 0.8 centered on the electron was required to be below 5 GeV. This requirement reduced photoproduction background;
- a track match with any electron falling in the range $0.3 < \theta < 2.6$, well within the CTD acceptance. For θ outside this region, $\delta > 44$ GeV was required. This cut further suppressed events from non-ep interaction and photoproduction;
- $y_{\rm JB} > 0.02$ to improve the accuracy of the DA reconstruction;
- $y_{\rm e} < 0.95$ to remove events where fake electrons were found in the FCAL;
- $Q^2_{\rm DA} > 25$ GeV^2.

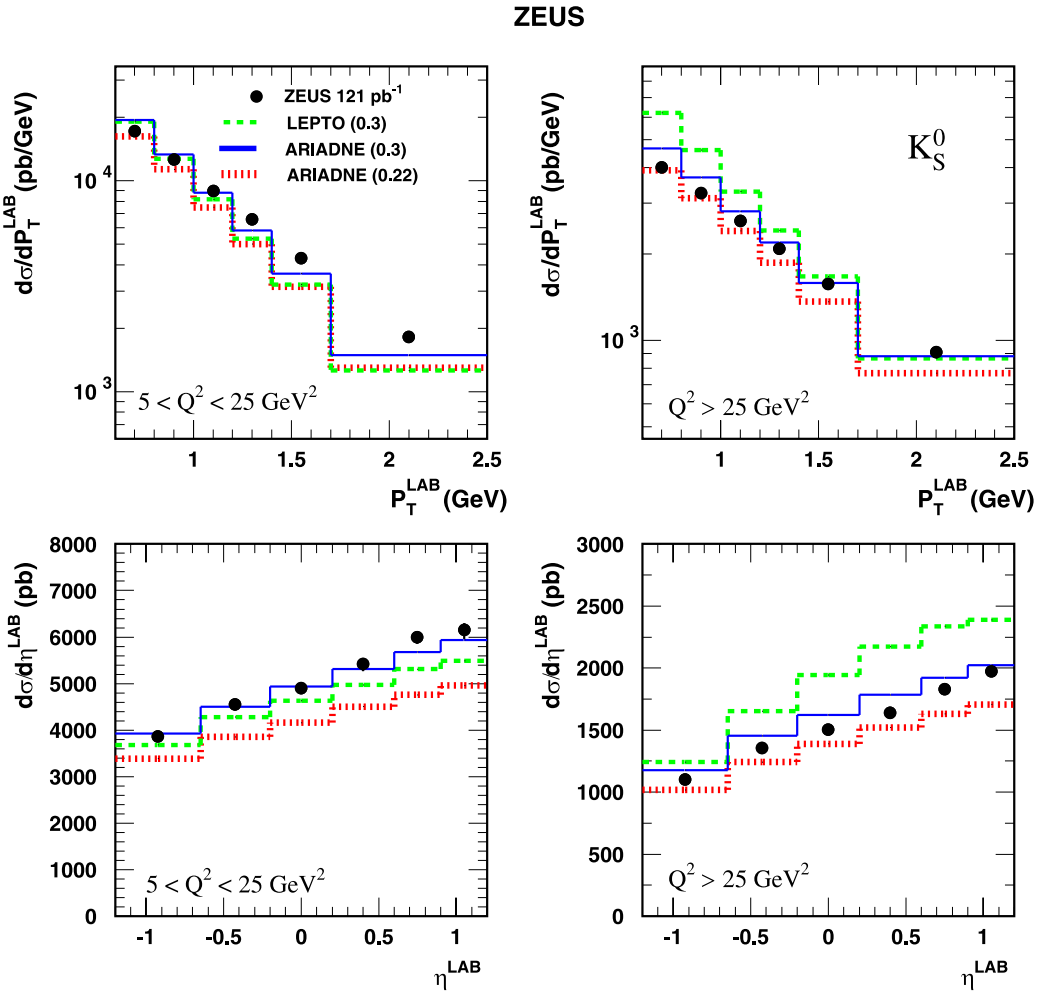

Fig. 3. Differential K^0_S cross-sections as a function of $P_{\rm T}^{\rm LAB}$ and $\eta^{\rm LAB}$ in the range $0.6 < P_{\rm T}^{\rm LAB} < 2.5$ GeV and $|\eta^{\rm LAB}| < 1.2$ for events with $5 < Q^2 < 25$ GeV^2, $0.02 < y < 0.95$ and $Q^2 > 25$ GeV^2, $0.02 < y < 0.95$. Statistical errors (inner error bars) and the systematic uncertainties added in quadrature are shown, unless smaller than the point size. The histograms show predictions from ARIADNE and LEPTO using the stated strangeness suppression

The same selection was used to obtain the low-Q^2 DIS sample, except for the Q^2 requirement and the position of the scattered electron, which were as follows:

- the impact position of the scattered electron on the CAL was required to be outside a rectangle of dimensions $26 \times 14\,\mathrm{cm}^2$, centred on the beam pipe;
- $5 < Q^2_{\mathrm{DA}} < 25\,\mathrm{GeV}^2$.

The trigger for selecting low-Q^2 events was normally prescaled, so the data correspond to an integrated luminosity of $16.6\,\mathrm{pb}^{-1}$.

It should be noted that there was no jet requirement in the DIS event samples.

3.2 Photoproduction sample

Photoproduction events were selected applying the following criteria, described in an earlier publication [55]:

- $|Z_{\mathrm{vtx}}| < 50\,\mathrm{cm}$, to reduce background from non-ep collisions;
- $y_{\mathrm{JB}} > 0.2$, to further reduce background from non-ep collisions;
- events were removed where an electron was found with $y_{\mathrm{e}} < 0.85$, reducing the background from neutral current DIS events;
- $y_{\mathrm{JB}} < 0.85$, to reduce background from neutral current DIS events where the electron was not identified;
- charged current DIS events were removed by rejecting events with $P_{\mathrm{T}}^{\mathrm{miss}}/\sqrt{E_{\mathrm{T}}} > 2.0\,\mathrm{GeV}^{\frac{1}{2}}$, where $P_{\mathrm{T}}^{\mathrm{miss}}$ is the missing transverse momentum and E_{T} is the total transverse energy.

Energy flow objects, reconstructed from a combination of calorimeter and tracking information to give the best resolution of kinematic variables, were used as the input to the k_{T} cluster jet-finding algorithm [65, 66], which was run in the longitudinally invariant inclusive mode [67]. The transverse energy of the jets was corrected for energy losses in inactive material in front of the CAL, as described in a previous publication [68]. An event was accepted if it

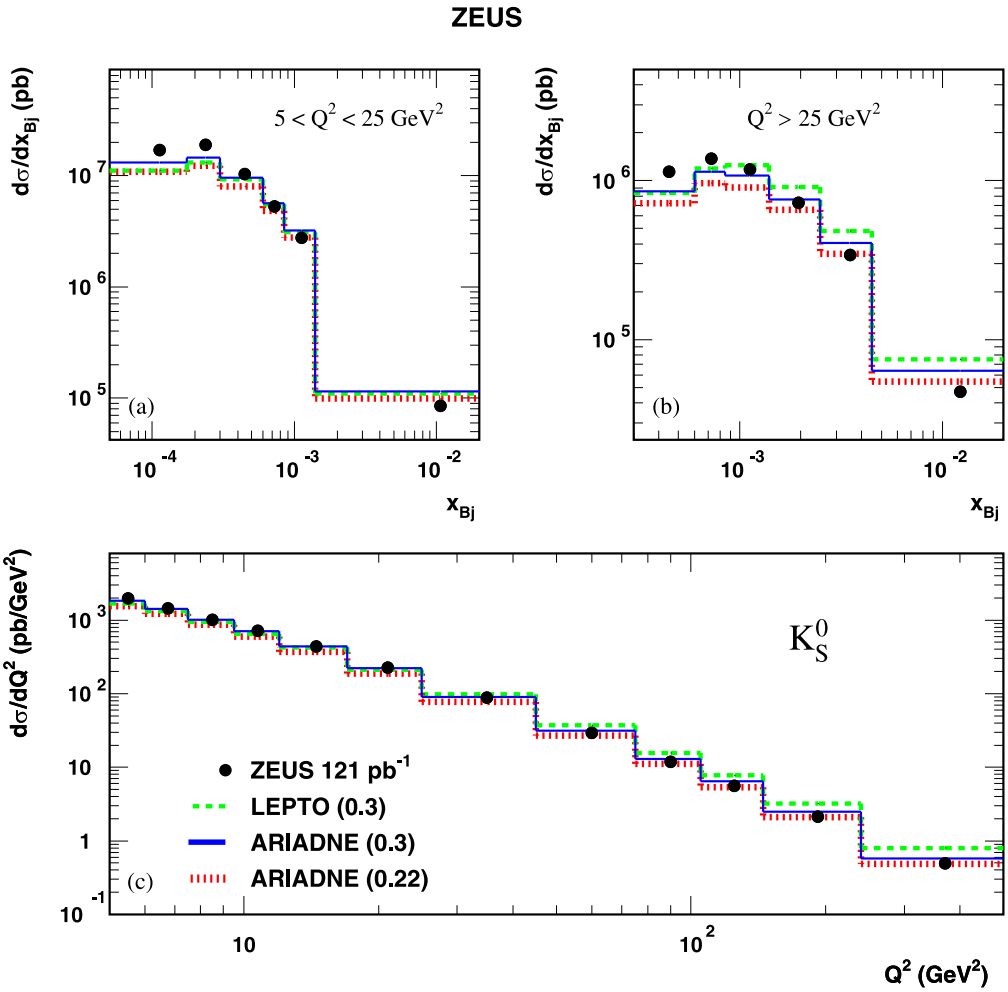

Fig. 4. Differential K^0_S cross sections as a function of x_{Bj} and Q^2 in the range $0.6 < P_{\mathrm{T}}^{\mathrm{LAB}} < 2.5$ GeV and $|\eta^{\mathrm{LAB}}| < 1.2$ for events **a** with $5 < Q^2 < 25\,\mathrm{GeV}^2$, $0.02 < y < 0.95$ **b** $Q^2 > 25\,\mathrm{GeV}^2$, $0.02 < y < 0.95$ and **c** $Q^2 > 5\,\mathrm{GeV}^2$, $0.02 < y < 0.95$. Statistical errors and the systematic uncertainties added in quadrature are smaller than the point size. The histograms show predictions from ARIADNE and LEPTO using the stated strangeness suppression

contained at least two jets, both satisfying the following criteria:

– jet transverse energy $E_{\rm T}^{\rm jet} > 5$ GeV;
– jet pseudorapidity $|\eta^{\rm jet}| < 2.4$.

Photoproduction events selected in this way contributed about 10% to the total photoproduction cross section. The photoproduction sample was divided into subsamples using the variable $x_\gamma^{\rm OBS}$, a measure of the fraction of the photon energy transferred to the dijet system, defined as:

$$x_\gamma^{\rm OBS} = \frac{\sum E_{\rm T}^{\rm jet} {\rm e}^{-\eta^{\rm jet}}}{2 y_{\rm JB} E_{\rm e}^{\rm beam}},$$

where the sum runs over the two jets with highest transverse energy. In leading-order QCD, $x_\gamma^{\rm OBS} = 1$ corresponds to direct photon processes in which the photon takes part in the hard scattering as a point-like particle. Resolved photon processes, in which the photon acts as a source of partons, populate the region at $x_\gamma^{\rm OBS} < 1$. The sample with $x_\gamma^{\rm OBS} > 0.75$ is classified as direct-enriched, and that with $x_\gamma^{\rm OBS} < 0.75$ as resolved-enriched.

3.3 Strange particle reconstruction

Candidates for long-lived neutral strange hadrons decaying to two charged particles were identified by selecting pairs of oppositely charged tracks, fitted to a displaced secondary vertex. Events were required to have at least one such candidate. These secondary vertices were found by the ZEUS track-finding software, which is based on minimizing the χ^2 arising from fitting tracks to vertices [69]. Displaced vertices were typically more than 3 cm away from the primary vertex. The minimal distance required to resolve a displaced vertex from the primary vertex was about 1 cm. The tracks fitted to this vertex were required to pass through at least the fifth superlayer of the CTD, the transverse momentum was required to be greater than 150 MeV and the absolute pseudorapidity in the laboratory frame was re-

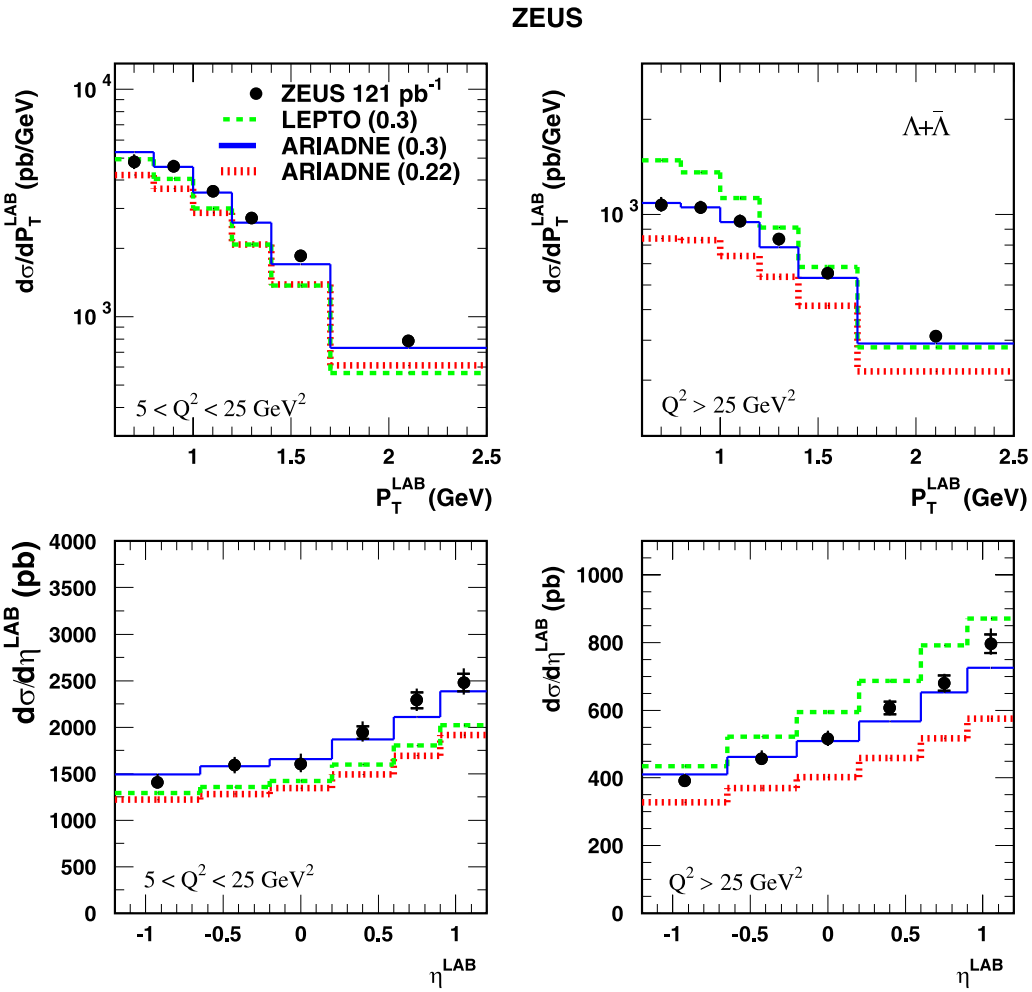

Fig. 5. Differential $\Lambda + \bar{\Lambda}$ cross sections as a function of $P_{\rm T}^{\rm LAB}$ and $\eta^{\rm LAB}$ in the range $0.6 < P_{\rm T}^{\rm LAB} < 2.5$ GeV and $|\eta^{\rm LAB}| < 1.2$ for events with $5 < Q^2 < 25$ GeV^2, $0.02 < y < 0.95$ and $Q^2 > 25$ GeV^2, $0.02 < y < 0.95$. Statistical errors (inner error bars) and the systematic uncertainties added in quadrature are shown, unless smaller than the point size. The histograms show predictions from ARIADNE and LEPTO using the stated strangeness suppression

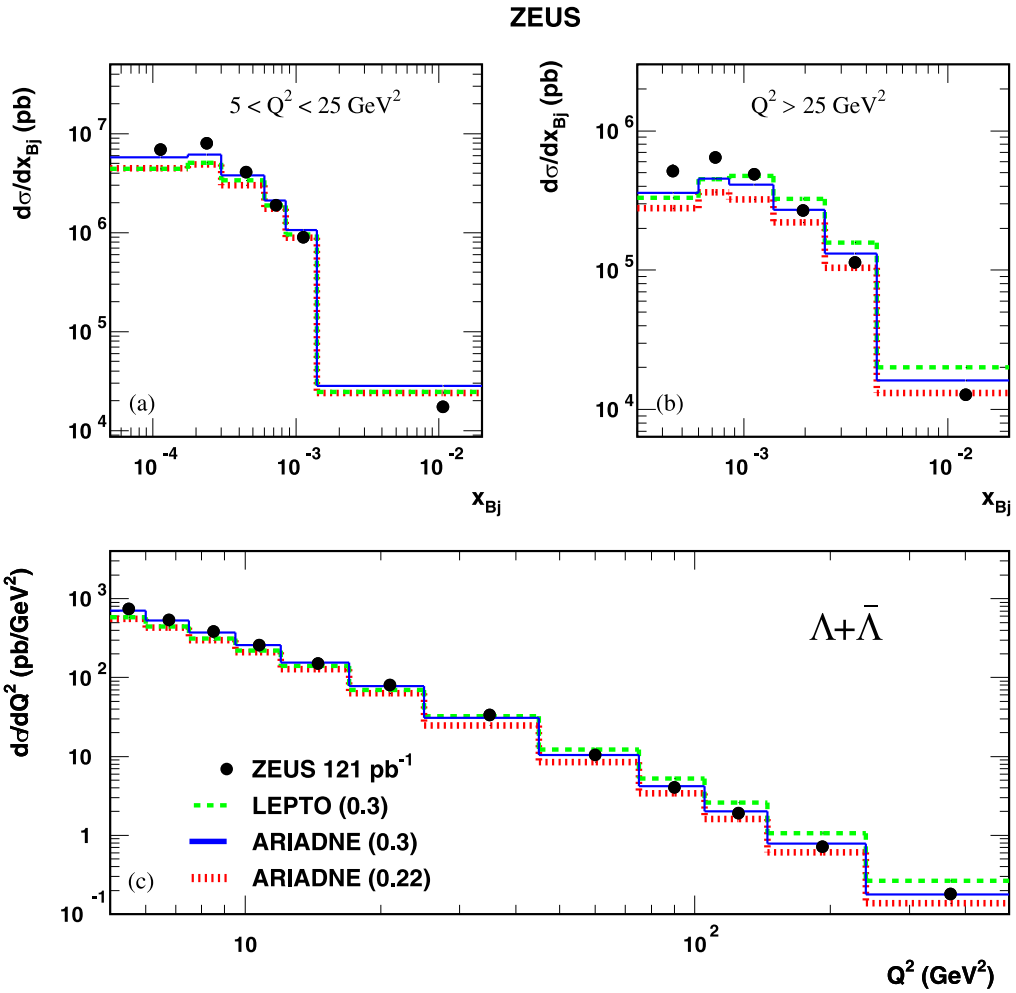

Fig. 6. Differential $\Lambda+\bar{\Lambda}$ cross sections as a function of $x_{\rm Bj}$ and Q^2 in the range $0.6 < P_{\rm T}^{\rm LAB} < 2.5$ GeV and $|\eta^{\rm LAB}| < 1.2$ for events **a** with $5 < Q^2 < 25$ GeV^2, $0.02 < y < 0.95$ **b** $Q^2 > 25$ GeV^2, $0.02 < y < 0.95$ and **c** $Q^2 > 5$ GeV^2, $0.02 < y < 0.95$. Statistical errors and the systematic uncertainties added in quadrature are smaller than the point size. The histograms show predictions from ARIADNE and LEPTO using the stated strangeness suppression

quired to be less than 1.5. These constraints ensured a good track resolution and acceptance. The Λ, $\bar{\Lambda}$ and K^0_S particles may also be created in interactions with the beam pipe. To remove these events a collinearity cut on the angle between the reconstructed candidate momentum and the vector joining the primary vertex to secondary vertex was applied. This angle was restricted to be less than 0.2.

The $\Lambda(\bar{\Lambda})$ candidates were reconstructed by their charged decay mode to $p\pi^-$ ($\bar{p}\pi^+$) (branching ratio $63.9 \pm 0.5\%$ [70]). The track with the larger momentum was assigned the mass of the proton, while the other was assigned the mass of the charged pion, as the decay proton always has a larger momentum than the pion, provided the $\Lambda(\bar{\Lambda})$ momentum is greater than 0.3 GeV. Additional requirements to select $\Lambda(\bar{\Lambda})$ are given in the following:

- $0.6 < P_{\rm T}^{\rm LAB}(\Lambda, \bar{\Lambda}) < 2.5$ GeV, where $P_{\rm T}^{\rm LAB}(\Lambda, \bar{\Lambda})$ is the transverse momentum of the reconstructed candidate;
- $|\,\eta^{\rm LAB}(\Lambda, \bar{\Lambda})\,| < 1.2$, where $\eta^{\rm LAB}(\Lambda,\ \bar{\Lambda})$ is the pseudorapidity of the reconstructed candidate in the laboratory;
- $M(e^+e^-) > 0.05$ GeV, to eliminate electron pairs from photon conversions[4];
- $M(\pi^+\pi^-) < 0.475$ GeV, to remove K^0_S contamination;
- $1.11 < M(p\pi) < 1.122$ GeV.

The K^0_S meson candidates were reconstructed from the decays to $\pi^+\pi^-$ (branching ratio $68.95 \pm 0.14\%$ [70]). Both tracks were assigned the mass of the charged pion. Additional requirements to select K^0_S are given in the following:

- $0.6 < P_{\rm T}^{\rm LAB}(K^0_S) < 2.5$ GeV, where $P_{\rm T}^{\rm LAB}(K^0_S)$ is the transverse momentum of the reconstructed candidate;
- $|\,\eta^{\rm LAB}(K^0_S)\,| < 1.2$, where $\eta^{\rm LAB}(K^0_S)$ is the pseudorapidity of the reconstructed candidate in the laboratory;
- $M(e^+e^-) > 0.05$ GeV;
- $M(p\pi) > 1.125$ GeV, to remove Λ and $\bar{\Lambda}$ contamination. Here the mass of the proton was assigned to the track with larger momentum and the mass of the pion to the other track;
- $0.48 < M(\pi^+\pi^-) < 0.52$ GeV.

[4] $M(ab)$ is defined as the invariant mass for two vertex tracks with the assignment of masses of particles a and b.

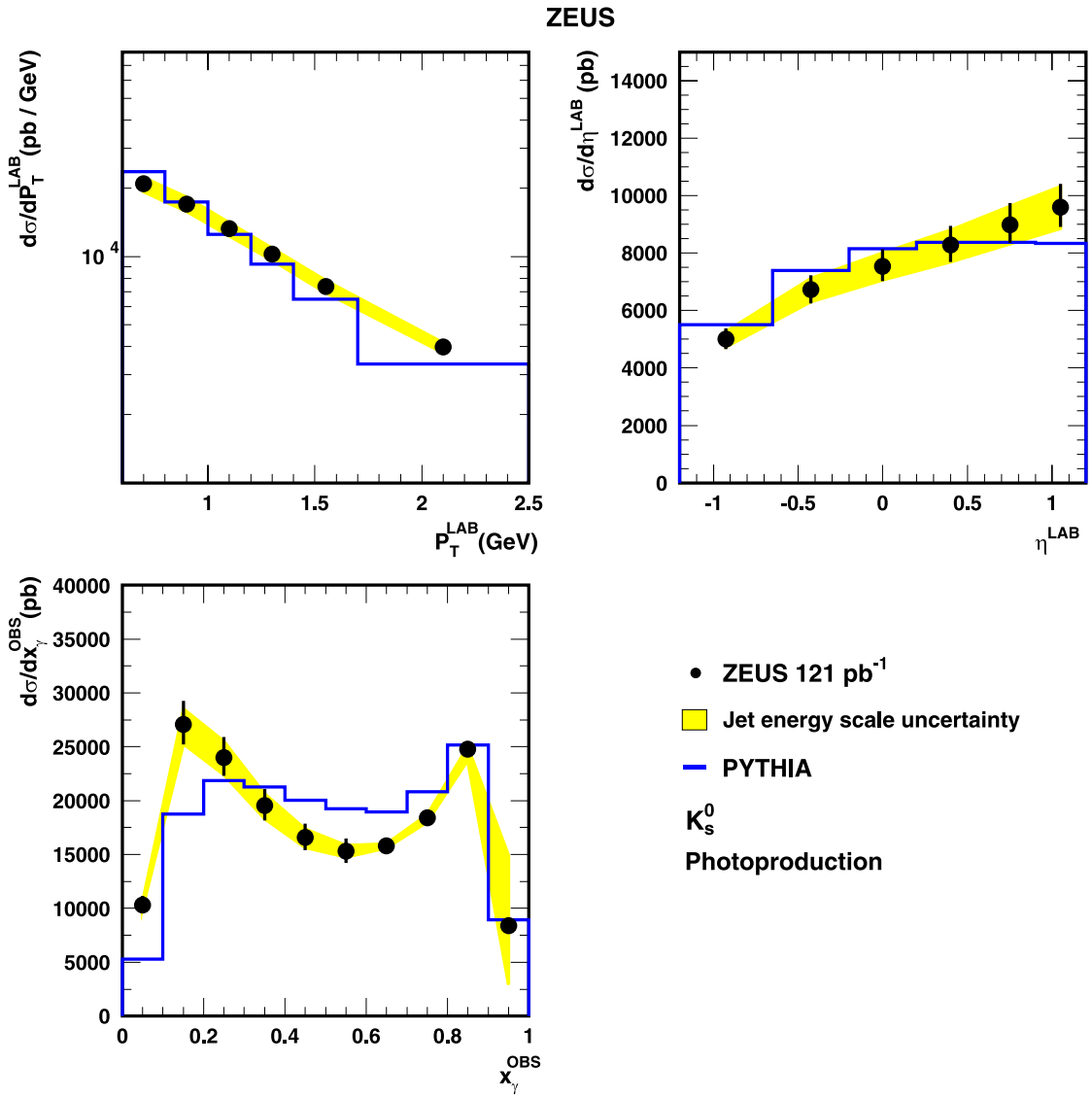

Fig. 7. Differential K^0_S cross sections as a function of $P_{\rm T}^{\rm LAB}$, $\eta^{\rm LAB}$ and $x_\gamma^{\rm OBS}$, in the range $0.6 < P_{\rm T}^{\rm LAB} < 2.5$ GeV and $|\eta^{\rm LAB}| < 1.2$ for events with $Q^2 < 1\,{\rm GeV}^2$, $0.2 < y < 0.85$ and at least two jets both satisfying $E_{\rm T}^{\rm jet} > 5$ GeV and $|\eta^{\rm jet}| < 2.4$. Statistical errors are shown, unless smaller than the point size, together with the systematic uncertainty arising from the trigger efficiency added in quadrature. The uncertainty arising from the jet energy scale is also shown (*shaded band*). The *solid histogram* shows the prediction from PYTHIA (with multiple interactions), normalised to the data

The mass peaks for K^0_S and $\Lambda + \bar{\Lambda}$ in the high-Q^2 sample are shown in Fig. 1. The decay of K^0_S, Λ, and $\bar{\Lambda}$ was well understood as can be demonstrated by Fig. 2, which shows the proper decay times, reconstructed from the three dimensional decay length, compared to the expectations from MC simulation (see below).

4 Event simulation

Production of K^0_S, Λ and $\bar{\Lambda}$ hadrons was modelled using the MC programs described below. In these models, strange quarks can be produced perturbatively by the boson–gluon fusion process ($\gamma g \to s\bar{s}$) or by gluon splitting in so-called parton showers. They may also originate from the proton parton densities or can be generated in non-perturbative string fragmentation. Strange hadrons are produced during hadronization, when quarks recombine into hadrons, and through the decays of other hadrons. Samples of events were generated to determine the response of the detector and obtain the correction factors required to convert the detector-level distributions to the hadron level. The generated events were passed through a full simulation of the detector, using GEANT 3.13 [71], and processed with the same reconstruction program as used for the data.

The high-Q^2 and the low-Q^2 DIS data were corrected to the hadron level using the ARIADNE 4 [25] MC program interfaced to HERACLES 4.6.1 [72–75] via DJANGOH 1.1[75], to include QED corrections. The CTEQ proton

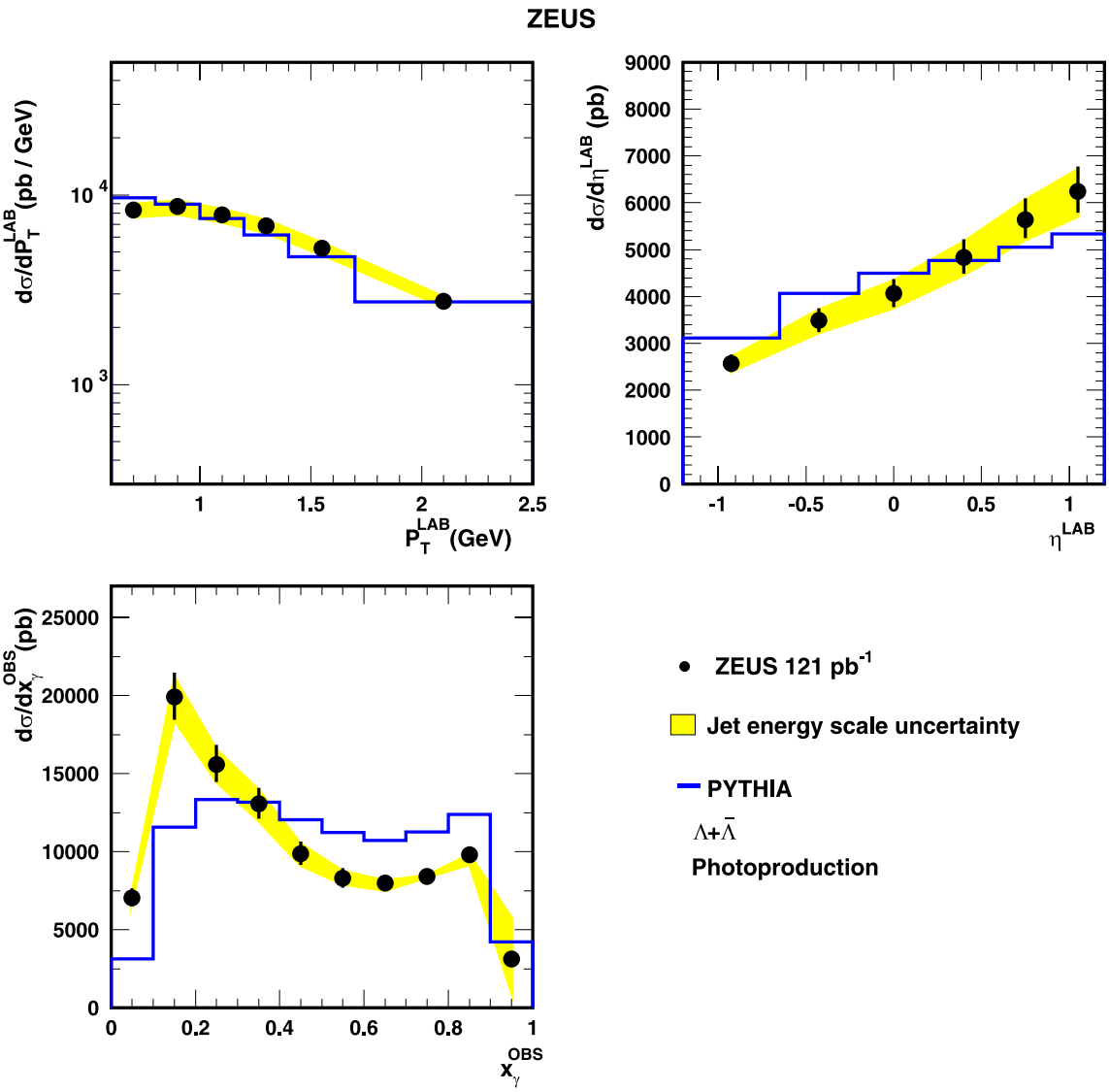

Fig. 8. Differential $\Lambda + \bar{\Lambda}$ cross sections as a function of $P_{\mathrm{T}}^{\mathrm{LAB}}$, η^{LAB} and x_γ^{OBS}, in the range $0.6 < P_{\mathrm{T}}^{\mathrm{LAB}} < 2.5\,\mathrm{GeV}$ and $|\eta^{\mathrm{LAB}}| < 1.2$ for events with $Q^2 < 1\,\mathrm{GeV}^2$, $0.2 < y < 0.85$ and at least two jets both satisfying $E_{\mathrm{T}}^{\mathrm{jet}} > 5\,\mathrm{GeV}$ and $|\eta^{\mathrm{jet}}| < 2.4$. Statistical errors are shown, unless smaller than the point size, together with the systematic uncertainty arising from the trigger efficiency added in quadrature. The uncertainty arising from the jet energy scale is also shown (*shaded band*). The *solid histogram* shows the prediction from PYTHIA (with multiple interactions), normalised to the data

parton density functions were used [76, 77]. ARIADNE is based on the colour dipole model in which most QCD coherence effects are modelled as gluon emission from colour dipoles between partons. The program uses the Lund string model [78] to simulate the fragmentation of the partons. A significant parameter governing the production of strange hadrons is the strangeness-suppression factor, λ_s, that is the probability to produce s-quark pairs relative to u- and d-quark pairs in the string fragmentation. This was set to 0.3, the default value, as found in e^+e^- annihilation [79–82]. Other parameters that control baryon production were set to their default values[5] [83]. This ARIADNE sample was also used to compare to the final cross sections and ratios.

A value of λ_s smaller than 0.3 is often preferred [12, 16–19, 84, 85] for K^0_S production. Therefore, a further sample with $\lambda_s = 0.22$ [86] was also generated and used for comparison. The DIS data were additionally simulated using the LEPTO 6.5 MC program [26], which is based on first-order matrix elements plus parton showers (MEPS). The

[5] The key parameters for baryon production in JETSET are the diquark–antidiquark pair production suppression PARJ(1) = 0.10, the suppression of s quark pair production compared to u or d pair production $\lambda_s \equiv$ PARJ(2) = 0.30, the extra suppression of strange diquark production compared with the normal suppression of strange quarks PARJ(3) = 0.4 and the suppression of spin 1 diquarks compared with spin 0 ones PARJ(4) = 0.05.

same Lund string model was used for the hadronisation, with $\lambda_s = 0.3$, and the same proton parton density functions as in the ARIADNE sample. This was used for further comparison to the data.

The photoproduction data were corrected to the hadron level using the PYTHIA 6 event generator [28], which consists of leading-order matrix-element calculations with initial- and final-state parton showering to simulate higher-order processes. The proton and photon PDFs were taken from GRV [87] and SaS2D [88], respectively. Multiple interactions [55, 89–93], where more than one pair of partons (one parton from the photon and one parton from the proton) interact independently, were included. The default implementation was used, with the $p_{\mathrm{T}}^{\mathrm{min}}$ [83] value of 2.7 GeV. The hadronisation is performed by the Lund string model, as in ARIADNE, with the same parameters controlling the production of strange hadrons. Direct and resolved events were generated separately. For correction of the data, the direct and resolved subsamples were combined such that they gave a best fit to the data x_γ^{OBS} distribution. The PYTHIA sample was also used to compare to the final cross sections and ratios, in which case the direct and resolved events were combined according to the predicted cross sections.

5 Cross-section determination

The cross sections in the high-Q^2 DIS sample were measured in the kinematic region $Q^2 > 25\,\mathrm{GeV}^2$ and $0.02 < y < 0.95$. The cross sections in the low-Q^2 DIS sample were measured in the kinematic region $5 < Q^2 < 25\,\mathrm{GeV}^2$ and $0.02 < y < 0.95$. The cross sections in the photoproduction sample were measured in the kinematic region $Q^2 < 1\,\mathrm{GeV}^2$ and $0.2 < y < 0.85$, with the additional requirement of 2 jets, both satisfying $E_{\mathrm{T}}^{\mathrm{jet}} > 5\,\mathrm{GeV}$ and $|\eta^{\mathrm{jet}}| < 2.4$. In all three samples there was a further kinematic requirement that $0.6 < P_{\mathrm{T}}^{\mathrm{LAB}}(K^0_S, \Lambda, \bar{\Lambda}) < 2.5\,\mathrm{GeV}$ and $|\eta^{\mathrm{LAB}}(K^0_S, \Lambda, \bar{\Lambda})| < 1.2$. In all samples the measured

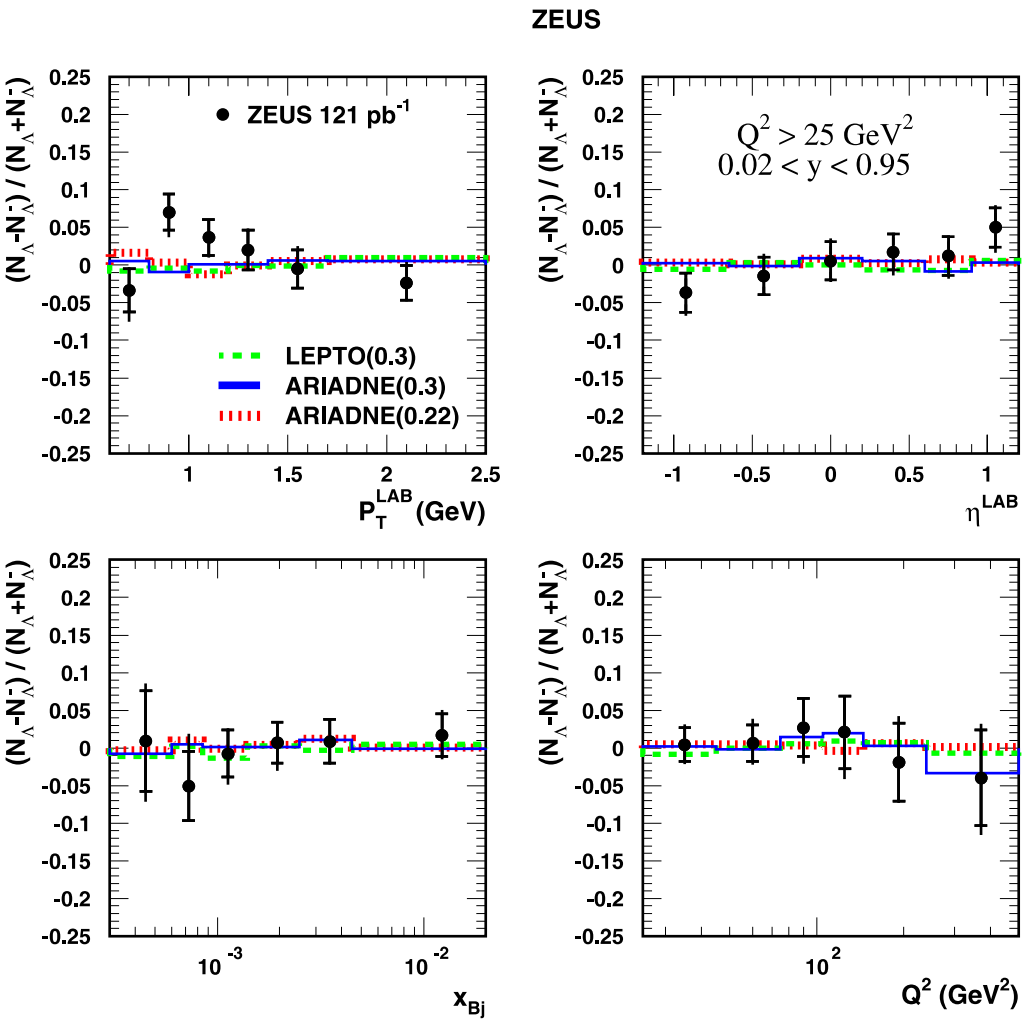

Fig. 9. The ratio $\frac{N(\Lambda)-N(\bar{\Lambda})}{N(\Lambda)+N(\bar{\Lambda})}$ as a function of $P_{\mathrm{T}}^{\mathrm{LAB}}$, η^{LAB}, x_{Bj} and Q^2, in the range $0.6 < P_{\mathrm{T}}^{\mathrm{LAB}} < 2.5\,\mathrm{GeV}$ and $|\eta^{\mathrm{LAB}}| < 1.2$ for events with $Q^2 > 25\,\mathrm{GeV}^2$ and $0.02 < y < 0.95$. Statistical errors (inner error bars) and the systematic uncertainties added in quadrature are shown. The histograms show predictions from ARIADNE and LEPTO using the stated strangeness suppression

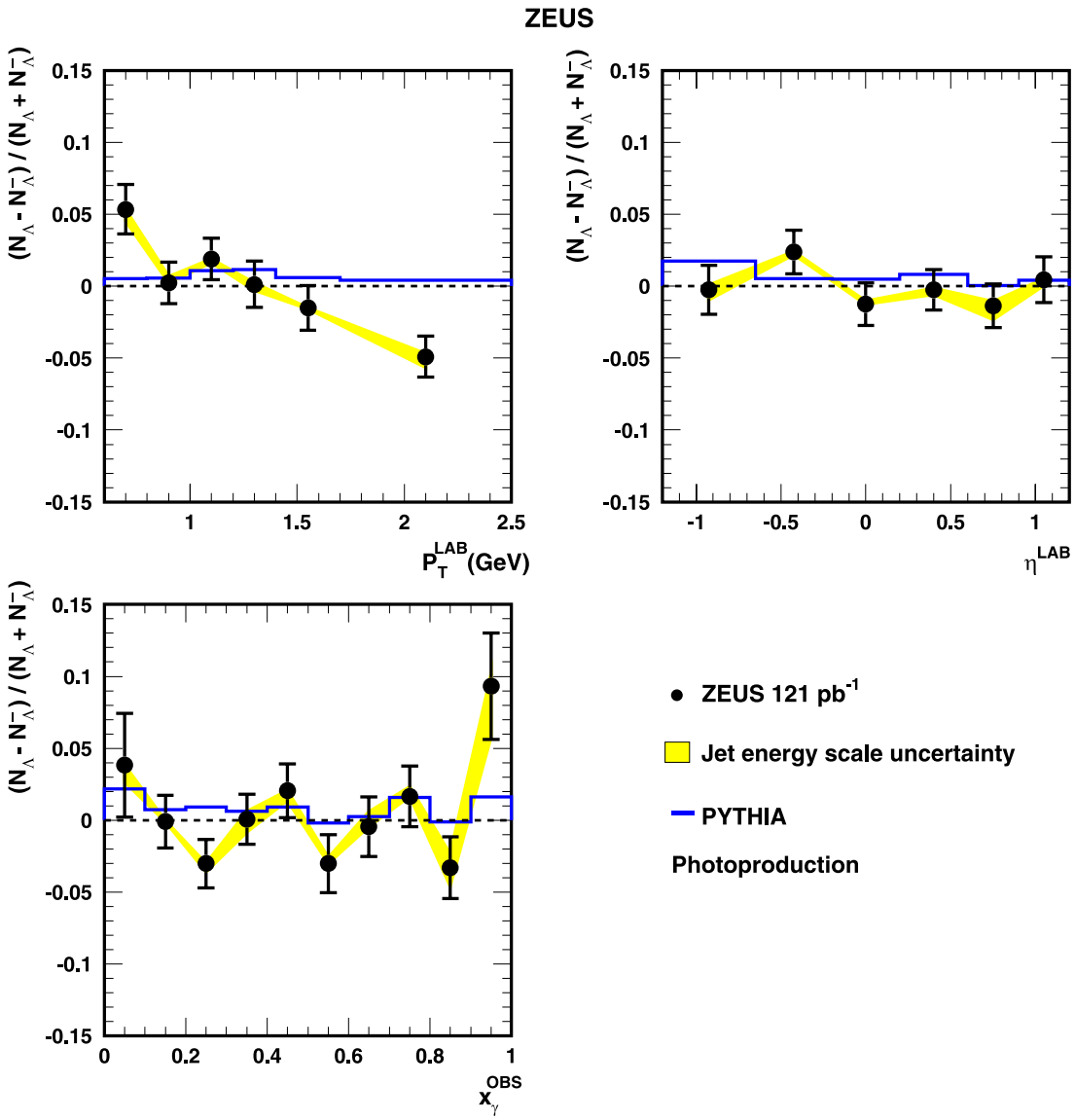

Fig. 10. The ratio $\frac{N(\Lambda)-N(\bar{\Lambda})}{N(\Lambda)+N(\bar{\Lambda})}$ as a function of $P_{\rm T}^{\rm LAB}$, $\eta^{\rm LAB}$ and $x_\gamma^{\rm OBS}$, in the range $0.6 < P_{\rm T}^{\rm LAB} < 2.5$ GeV and $|\eta^{\rm LAB}| < 1.2$ for events with $Q^2 < 1\,{\rm GeV}^2$, $0.2 < y < 0.85$ and at least two jets both satisfying $E_{\rm T}^{\rm jet} > 5$ GeV and $|\eta^{\rm jet}| < 2.4$. Statistical errors are shown, together with the uncertainty arising from the jet energy scale (*shaded band*). The *solid histogram* shows the prediction from PYTHIA (with multiple interactions)

cross sections were the luminosity-weighted average of the cross sections at the centre-of-mass energies $\sqrt{s} = 318$ GeV and $\sqrt{s} = 300$ GeV. In the DIS samples differential cross sections were measured as functions of $P_{\rm T}^{\rm LAB}(K^0_S, \Lambda, \bar{\Lambda})$, $\eta^{\rm LAB}(K^0_S, \Lambda, \bar{\Lambda})$, $x_{\rm Bj}$, and Q^2. In the photoproduction sample differential cross sections were measured as functions of $P_{\rm T}^{\rm LAB}(K^0_S, \Lambda, \bar{\Lambda})$, $\eta^{\rm LAB}(K^0_S, \Lambda, \bar{\Lambda})$, and $x_\gamma^{\rm OBS}$.

The K^0_S, Λ and $\bar{\Lambda}$ differential cross sections in any variable Y were calculated using a standard bin-by-bin correction as follows:

$$\frac{{\rm d}\sigma}{{\rm d}Y} = \frac{N}{A \cdot \mathcal{L} \cdot B \cdot \Delta Y}\,,$$

where N is the number of K^0_S, Λ or $\bar{\Lambda}$ in a bin of width ΔY, $\mathcal{L}$ is the luminosity, A is the acceptance and B is the branching ratio. The acceptance was calculated from the MC samples described in Sect. 4, and took into account migration effects and efficiencies for each bin. The acceptance for each particle was calculated for each bin of a 6×6 grid in $p_{\rm T}$ and η. An additional acceptance correction was made to obtain the differential cross sections as functions of variables other than $p_{\rm T}$ or η. In each bin a mass-sideband subtraction method was used to subtract the remaining combinatorial background in the K^0_S, Λ and $\bar{\Lambda}$ samples, which was at the level of $\sim 3\%$ in the K^0_S sample and $\sim 6\%$ in the Λ and $\bar{\Lambda}$ samples.

The differential cross sections, $\frac{{\rm d}\sigma}{{\rm d}Y}$, for the considered particle as a function of η and $P_{\rm T}$ can be converted into the multiplicity distribution $\frac{1}{{\rm d}\sigma_{\rm inc}}\frac{{\rm d}\sigma}{{\rm d}Y}$, where $\sigma_{\rm inc}$ is the inclu-

sive event cross section using the following factors: $\sigma_{\rm inc}^{-1} = 2.6 \times 10^{-5}\,{\rm pb}^{-1}$ for the high-Q^2 sample, $8.9 \times 10^{-6}\,{\rm pb}^{-1}$ for the low-Q^2 sample and $1.6 \times 10^{-5}\,{\rm pb}^{-1}$ for the photoproduction sample. On average, in the measured $P_{\rm T}$ and η region, for the high-Q^2 sample, there were about 0.017Λ (or $\bar{\Lambda}$) and 0.09 K^0_S per event. The corresponding multiplicities for the photoproduction sample were 0.077 for Λ (or $\bar{\Lambda}$) and 0.27 for K^0_S.

5.1 Systematic uncertainties

The main sources which contributed to the systematic uncertainty were investigated by changing the analysis procedure, as outlined below, and observing the difference from the primary result. The total systematic uncertainty in the DIS samples for each bin was calculated by adding the individual contributions from the different variations in quadrature. The following sources of systematic uncertainties were considered: the energy measurement of the scattered electron; the measurement of Q^2, δ, $Z_{\rm vtx}$ and y; measurements of secondary-track $p_{\rm T}$ and η; the removal of Λ and K^0_S due to the collinearity cut; the impact position of the electron on the CAL; the estimation of the background. The systematic uncertainty on the cross sections was generally $\lesssim 5\%$. Additionally, a 2% uncertainty due to the luminosity measurement was included for the cross sections. The branching-ratio uncertainties were deemed negligible and not taken into account.

The most significant systematic error in the photoproduction sample was due to the uncertainty in the calorimeter energy scale ($\pm 3\%$), shown as a separate band in the figures. Typical uncertainties in the cross sections were $\lesssim 10\%$, except in the highest bin of $x_\gamma^{\rm OBS}$ where the uncertainty was up to 80%. A systematic uncertainty of 7% on the photoproduction cross sections due to trigger efficiencies was included. The limitations of the PYTHIA Monte Carlo simulation, particularly in describing the $x_\gamma^{\rm OBS}$ distribution in the data, introduced a possible additional systematic uncertainty in correcting the data from detector level to hadron level. The effect of this was investi-

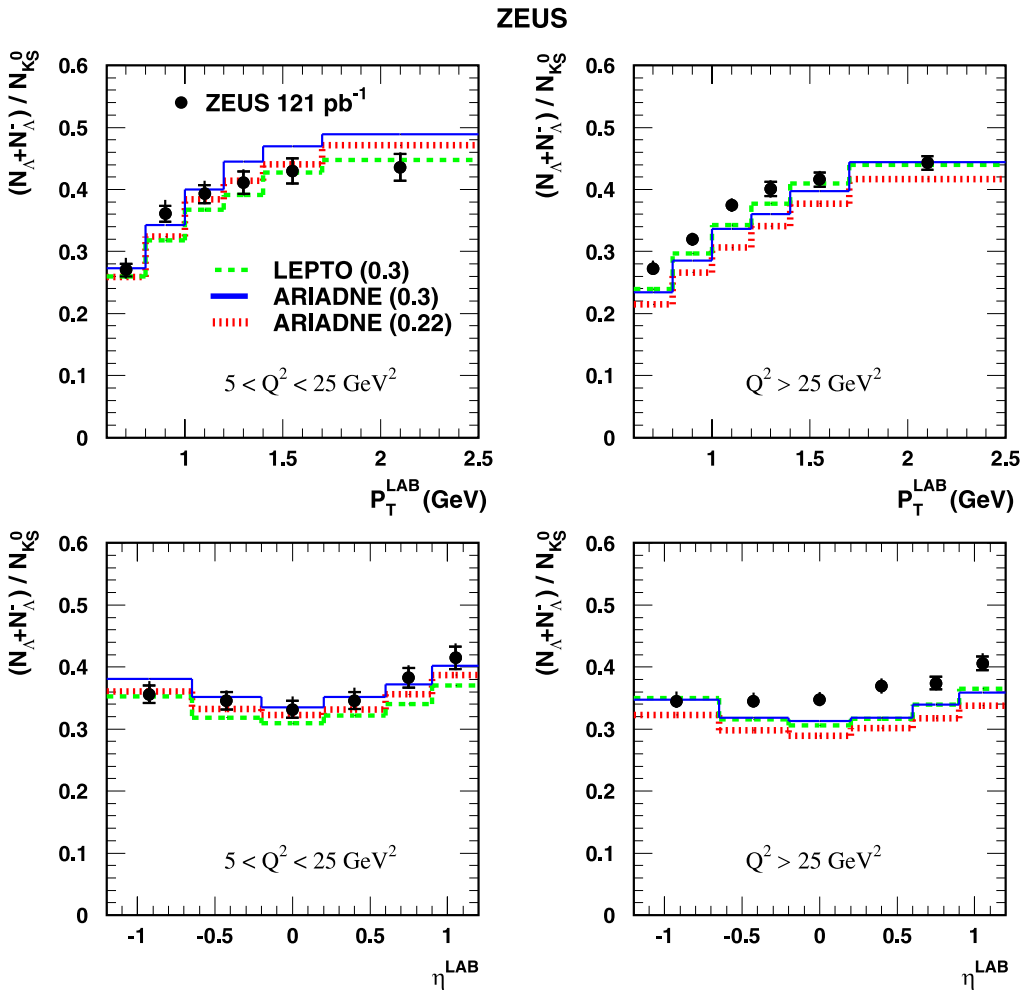

Fig. 11. The ratio $\frac{N(\Lambda)+N(\bar{\Lambda})}{N(K^0_S)}$ as a function of $P_{\rm T}^{\rm LAB}$ and $\eta^{\rm LAB}$ in the range $0.6 < P_{\rm T}^{\rm LAB} < 2.5$ GeV and $|\eta^{\rm LAB}| < 1.2$ for events with $5 < Q^2 < 25\,{\rm GeV}^2$, $0.02 < y < 0.95$ and $Q^2 > 25\,{\rm GeV}^2$, $0.02 < y < 0.95$. Statistical errors (inner error bars) and the systematic uncertainties added in quadrature are shown. The histograms show predictions from ARIADNE and LEPTO using the stated strangeness suppression

gated by reweighting the PYTHIA $x_\gamma^{\rm OBS}$ distribution to the data and using this reweighted sample to correct the data. The difference between the results obtained with the reweighted sample compared to the primary results was treated as a further systematic uncertainty; uncertainties in the cross sections were $\lesssim 5\%$.

The uncertainty of the tracking simulation [94] was negligible compared to all other sources. Most of the uncertainties discussed above cancel in the ratios and asymmetries presented in this paper.

6 Results and discussion

6.1 Cross sections

Measured differential cross sections for the production of K^0_S and $\Lambda + \bar{\Lambda}$ are shown in Figs. 3–6 for the DIS data and in Figs. 7 and 8 for the photoproduction sample. The DIS cross sections are compared to the absolute predictions of ARIADNE and LEPTO MC calculations. The photoproduction cross sections are compared to the prediction of the PYTHIA MC with multiple interactions normalised to the data cross section.

The ARIADNE program with strangeness-suppression factor of 0.3 describes the data reasonably well, although the K^0_S cross section for the high-Q^2 sample is overestimated. The slope of the $P_{\rm T}^{\rm LAB}$ dependence is incorrect and the cross section at low $x_{\rm Bj}$ is underestimated for both low- and high-Q^2 samples. A similar comment can be made for the $\Lambda + \bar{\Lambda}$ cross sections.

The description of the data by ARIADNE with the strangeness-suppression factor of 0.22 is less satisfactory but, as λ_s is not the only parameter influencing the cross section, a conclusion on what value of the λ_s can describe the data best cannot be drawn. The LEPTO MC does not describe the data well.

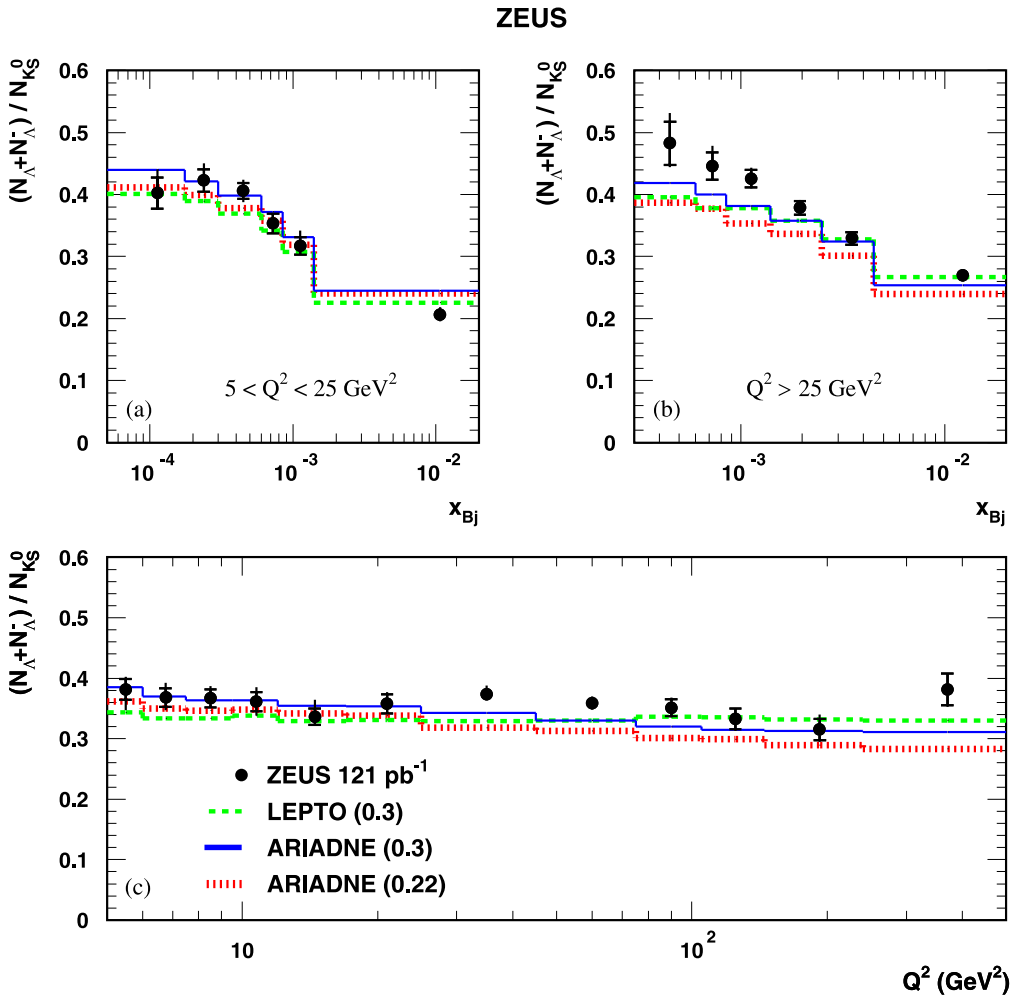

Fig. 12. The ratio $\frac{N(\Lambda)+N(\bar{\Lambda})}{N(K^0_S)}$ as a function of $x_{\rm Bj}$ and Q^2 in the range $0.6 < P_{\rm T}^{\rm LAB} < 2.5$ GeV and $|\eta^{\rm LAB}| < 1.2$ for events with **a** $5 < Q^2 < 25$ GeV^2, $0.02 < y < 0.95$ **b** $Q^2 > 25$ GeV^2, $0.02 < y < 0.95$ and **c** $Q^2 > 5$ GeV^2, $0.02 < y < 0.95$. Statistical errors (inner error bars) and the systematic uncertainties added in quadrature are shown. The histograms show predictions from ARIADNE and LEPTO using the stated strangeness suppression

In photoproduction, PYTHIA with multiple interactions describes the shape of the data dependence on $P_{\mathrm{T}}^{\mathrm{LAB}}$ and η^{LAB} adequately, but the x_γ^{OBS} dependence is predicted to be too flat and at the smallest x_γ^{OBS}, in the resolved photon region, the description is poor.

6.2 Baryon–antibaryon asymmetry

The baryon–antibaryon asymmetry $\mathcal{A}$ is defined as:

$$\mathcal{A} = \frac{N(\Lambda) - N(\bar{\Lambda})}{N(\Lambda) + N(\bar{\Lambda})},$$

where $N(\Lambda)$, $N(\bar{\Lambda})$ is the number of Λ and $\bar{\Lambda}$ baryons, respectively.

The baryon–antibaryon asymmetry $\mathcal{A}$ has been measured and compared to MC predictions from ARIADNE and PYTHIA (with $\lambda_s = 0.3$ for both, and also with $\lambda_s = 0.22$ for ARIADNE). The following values were obtained:

- at high Q^2: $\mathcal{A} = 0.3 \pm 1.3^{+0.5}_{-0.8}\%$, compared to the ARIADNE ($\lambda_s = 0.3$) prediction of $0.4 \pm 0.2\%$;
- at low Q^2: $\mathcal{A} = 1.2 \pm 1.6^{+0.7}_{-2.1}\%$, compared to the ARIADNE ($\lambda_s = 0.3$) prediction of $1.0 \pm 0.2\%$;
- in photoproduction: $\mathcal{A} = -0.07 \pm 0.6^{+1.0}_{-1.0}\%$, compared to the PYTHIA prediction of $0.6 \pm 0.1\%$.

Figures 9 and 10 show the baryon–antibaryon asymmetry at high-Q^2 as a function of $P_{\mathrm{T}}^{\mathrm{LAB}}$, η^{LAB}, x_{Bj}, Q^2 and in photoproduction as a function of $P_{\mathrm{T}}^{\mathrm{LAB}}$, η^{LAB} and x_γ^{OBS}. In all cases, the average baryon–antibaryon asymmetry is consistent both with no asymmetry and consistent with the very small asymmetry predicted by Monte Carlo. This suggests that in the considered parts of the ep phase-space, to a good approximation, baryons and antibaryons are produced according to the same mechanism.

A positive asymmetry of 3.5% is predicted in DIS [30], due to the so called gluon-junction mechanism that makes it possible for the "baryon number to travel" several units of rapidity, in this case from the proton beam direction to the rapidity around 0 in the laboratory frame in which the measurements were made. Such a class of models can describe the significant positive baryon–antibaryon asymmetry which has been measured at the heavy-ion collider RHIC [95]. Although this prediction is not Q^2 dependent, it is not clear whether it could be extended down to $Q^2 = 0$ and applied to the selected photoproduction sample. Combining statistical and systematic errors from the three samples, the average asymmetry is in disagreement with the 3.5% value.

Although ARIADNE predicts that on average about 15% (40% at the highest x_{Bj} for the low-Q^2 sample) of

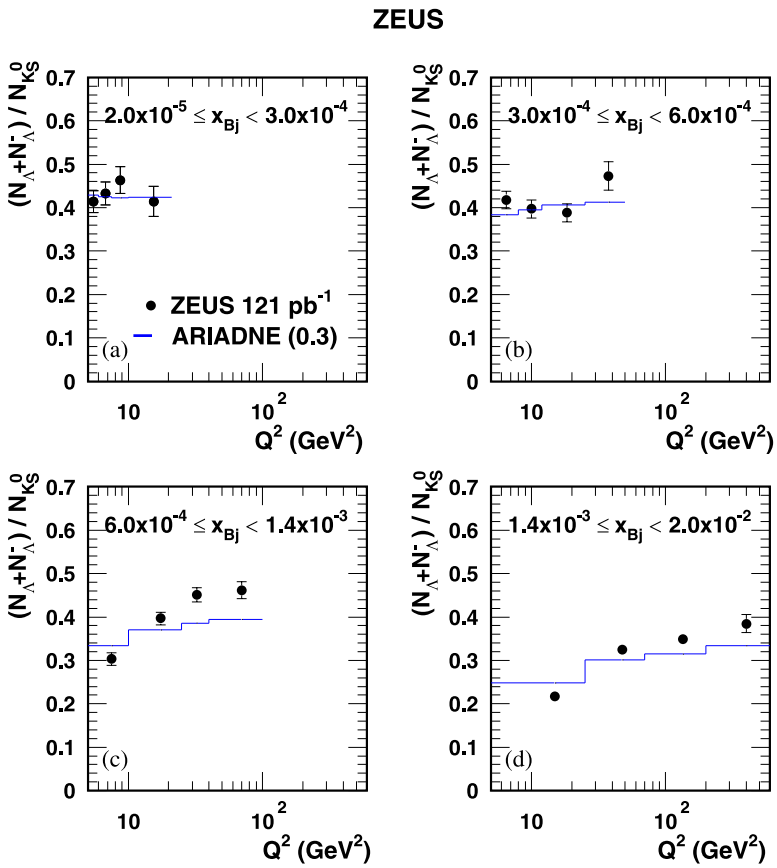

Fig. 13. The ratio $\frac{N(\Lambda)+N(\bar{\Lambda})}{N(K^0_S)}$ as a function of Q^2 for four bins of x_{Bj}, in the range $0.6 < P_{\mathrm{T}}^{\mathrm{LAB}} < 2.5$ GeV and $|\eta^{\mathrm{LAB}}| < 1.2$ for events with $Q^2 > 5$ GeV^2 and $0.02 < y < 0.95$. Statistical errors only are shown. The histograms show predictions from ARIADNE with a strangeness-suppression factor of 0.3

events with a reconstructed Λ or $\bar{\Lambda}$ originate from the exchanged photon coupling to an s or $\bar{s}$ quark from the proton, this measurement, being at low $x_{\rm Bj}$, is not sensitive to the strange-quark asymmetry in the proton structure function as studied by NuTeV [96].

As our baryon–antibaryon asymmetry is consistent with no asymmetry, the Λ and $\bar{\Lambda}$ samples were combined together (except for the transverse polarization measurement) and results presented for the combined sample.

6.3 Baryon-to-meson ratio

The baryon-to-meson ratio $\mathcal{R}$ is defined as:

$$\mathcal{R} = \frac{N(\Lambda)+N(\bar{\Lambda})}{N(K^0_S)},$$

where $N(\Lambda), N(\bar{\Lambda}), N(K^0_S)$ refer to the number of indicated hadrons.

Figures 11 and 12 show the measured and predicted $\mathcal{R}$ for the DIS samples as a function of $P_{\rm T}^{\rm LAB}$, $\eta^{\rm LAB}$, $x_{\rm Bj}$ and Q^2. The inaccuracies in describing the K^0_S and $\Lambda+\bar{\Lambda}$ cross sections for high Q^2, mentioned earlier, are clearly reflected in $\mathcal{R}$, but overall the ARIADNE MC with $\lambda_s = 0.3$ follows the shape of the data distributions and is usually in agreement to better than about 10%. The low-Q^2 sample is described by the same Monte Carlo programs with even better accuracy. In order to have a better understanding of how $\mathcal{R}$ depends on $x_{\rm Bj}$ and Q^2, $\mathcal{R}$ is shown as a function of Q^2 for fixed bins in $x_{\rm Bj}$ and as a function of $x_{\rm Bj}$ for fixed bins in Q^2 in Figs. 13 and 14. A dependence on Q^2 and a discrepancy between the data and MC can now be seen for the bins of higher $x_{\rm Bj}$. For the two bins of higher Q^2, the MC underestimates the data at low $x_{\rm Bj}$ by up to 20%. The $\mathcal{R}$ value varies between about 0.2 and 0.5, and is about 0.4 to 0.5 at low $x_{\rm Bj}$ and low Q^2. These values can be compared to measurements at e^+e^- colliders, where for centre-of-mass energies from 10 to 200 GeV, $\mathcal{R}$ varies between about 0.2 and 0.4 [70].

Figure 15 shows $\mathcal{R}$ for the photoproduction sample. For the direct-enriched sample, where $x_\gamma^{\rm OBS} > 0.75$, $\mathcal{R}$ is about 0.4, the same value as in DIS at low $x_{\rm Bj}$ and low Q^2. However, $\mathcal{R}$ rises to a value of about 0.7 towards low $x_\gamma^{\rm OBS}$ (resolved-enriched sample), while it stays flat in the PYTHIA prediction.

In order to study this effect further, the photoproduction events were divided into two samples. In the first, the jet with the highest transverse energy was required to contribute at most 30% to the total hadronic transverse

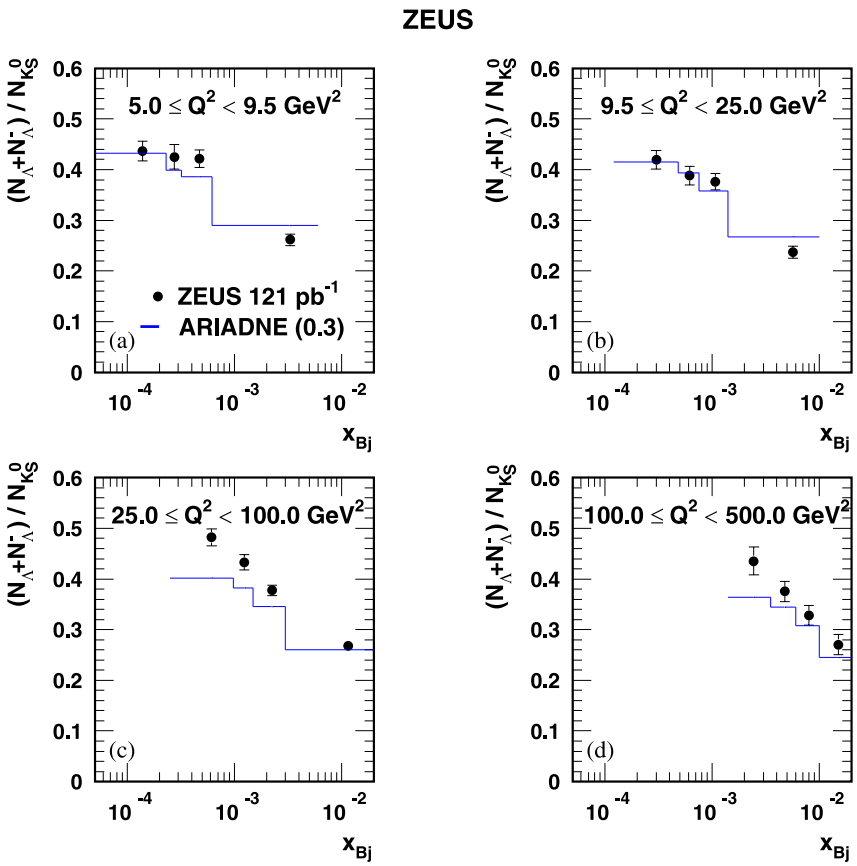

Fig. 14. The ratio $\frac{N(\Lambda)+N(\bar{\Lambda})}{N(K^0_S)}$ as a function of $x_{\rm Bj}$ for four bins of Q^2, in the range $0.6 < P_{\rm T}^{\rm LAB} < 2.5$ GeV and $|\eta^{\rm LAB}| < 1.2$ for events with $Q^2 > 5$ GeV^2 and $0.02 < y < 0.95$. Statistical errors only are shown. The histograms show predictions from ARIADNE with a strangeness-suppression factor of 0.3

energy. In this sample the events have largely isotropic transverse energy flow and therefore the sample is called "fireball-enriched". The other sample, containing all the other events, was called "fireball-depleted". Figure 16a shows the distribution of events as a function of the total transverse energy, which is on average 30 GeV, and of the transverse energy of the jet with the highest $E_{\rm T}^{\rm jet}$. The line represents the cut used to separate fireball-enriched and fireball-depleted samples. Figure 16b illustrates the fireball selection in relation to the fraction of the total transverse energy carried by two jets of the highest transverse energy. It can be seen that fireball-depleted events are dominated by dijet events carrying most of the total transverse energy and that the fireball-enriched and fireball-depleted samples have about the same number of events.

The baryon-to-meson ratios for the fireball-enriched and fireball-depleted samples are presented in Fig. 17 for the data and PYTHIA MC. The measured $\mathcal{R}$ is larger for the fireball-enriched sample, most significantly at high $P_{\rm T}^{\rm LAB}$, than it is for the fireball-depleted sample. This feature is not reproduced by PYTHIA, which predicts almost the same $\mathcal{R}$ for both samples. The PYTHIA prediction reasonably describes the measured values of $\mathcal{R}$ for the fireball-depleted sample. This is not surprising as PYTHIA generates jets in events according to the multiple interaction mechanism [89–92], which makes several independent jets, like those in DIS or e^+e^- where baryons and mesons are created locally. Provided there is enough energy available, $\mathcal{R}$ will be the same, regardless of the number of jets (ignoring some differences in quark and gluon fragmentation).

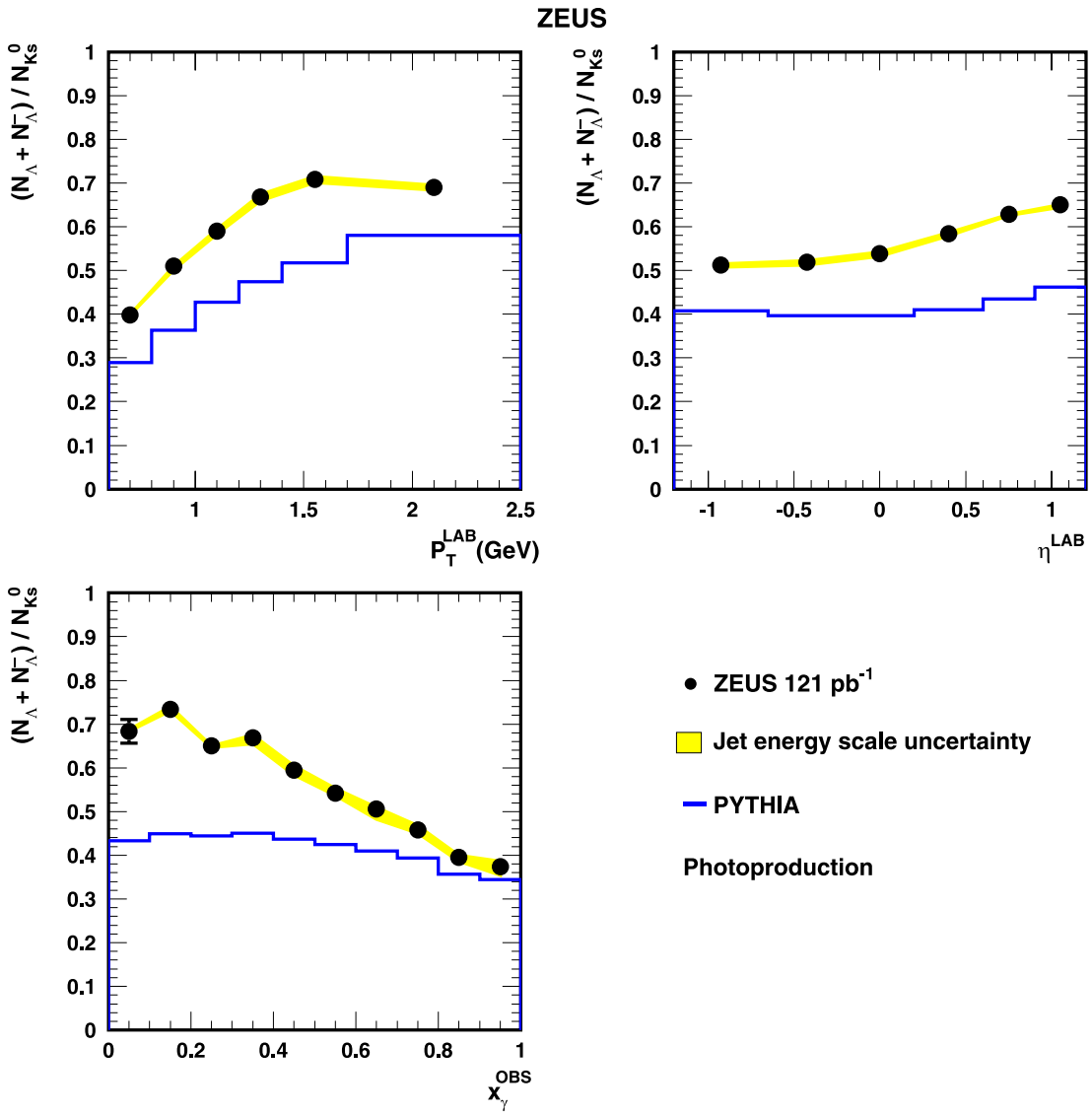

Fig. 15. The ratio $\frac{N(\Lambda)+N(\bar{\Lambda})}{N(K^0_S)}$ as a function of $P_{\rm T}^{\rm LAB}$, $\eta^{\rm LAB}$ and $x_\gamma^{\rm OBS}$, in the range $0.6 < P_{\rm T}^{\rm LAB} < 2.5$ GeV and $|\eta^{\rm LAB}| < 1.2$ for events with $Q^2 < 1$ GeV^2, $0.2 < y < 0.85$ and at least two jets both satisfying $E_{\rm T}^{\rm jet} > 5$ GeV and $|\eta^{\rm jet}| < 2.4$. The statistical errors are shown, unless smaller than the point size. The *shaded band* shows the uncertainty arising from the jet energy scale. The *solid histogram* shows the prediction from PYTHIA (with multiple interactions)

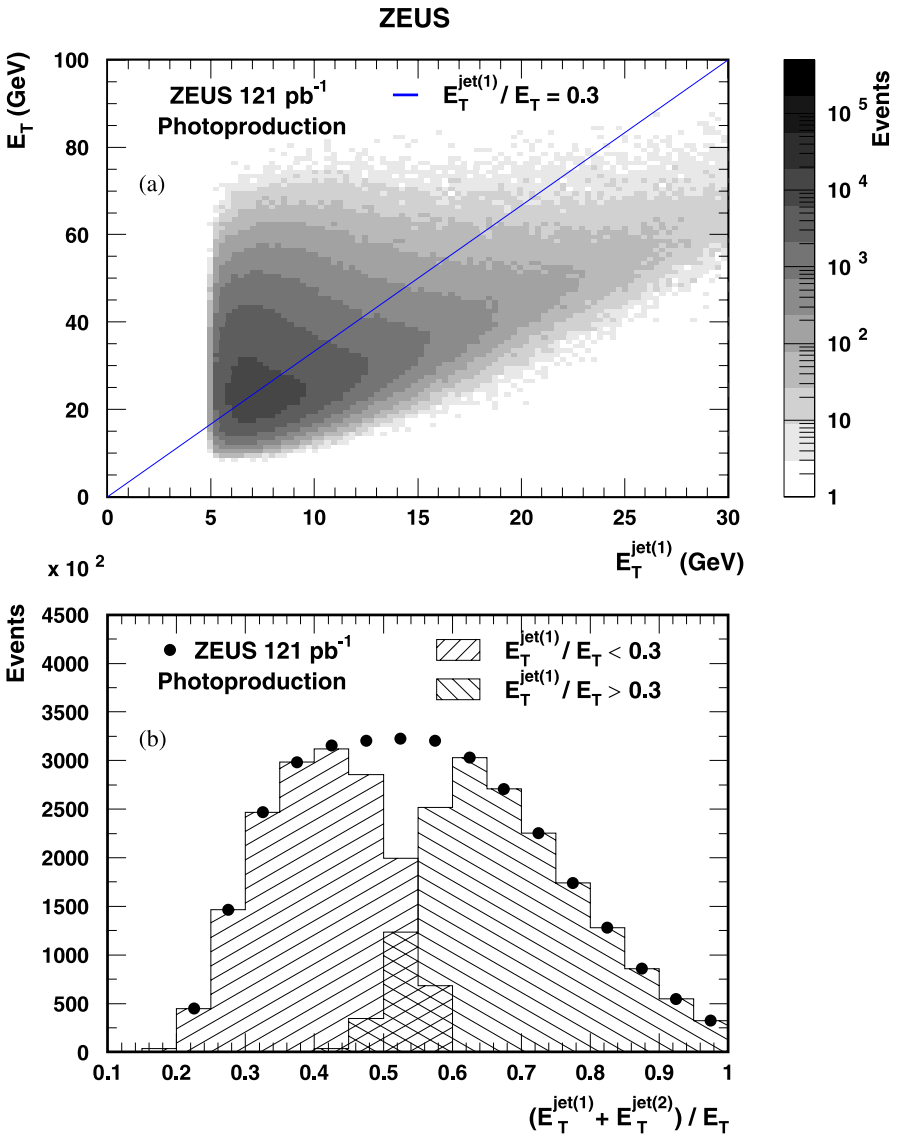

Fig. 16. **a** Distribution of photoproduction events as a function of the total transverse energy and the transverse energy of the jet with the highest transverse energy. Here the event sample was selected without any strange hadron requirements. The *solid line* represents the cut used to separate fireball-enriched and fireball-depleted subsamples. **b** The fraction of the total E_{T} carried by the two jets of highest transverse energy for the same data sample as in **a**. Fireball-enriched ($E_{\mathrm{T}}^{\mathrm{jet}(1)}/E_{\mathrm{T}} < 0.3$) and fireball-depleted ($E_{\mathrm{T}}^{\mathrm{jet}(1)}/E_{\mathrm{T}} > 0.3$) samples are shown. Statistical errors are smaller than the point size

Large values of $\mathcal{R}$, larger than 1, have been measured at hadron and heavy-ion colliders: $p\bar{p}$ [23], pp [24, 97] and RHIC [98–101].

6.4 Ratio of strange-to-light hadrons

The ratio of strange-to-light hadrons was measured in terms of $\mathcal{T}$:

$$\mathcal{T} = \frac{N(K^0_S)}{N_{\mathrm{ch}}},$$

where $N(K^0_S)$ is the number of K^0_S and N_{ch} is the number of charged pions, charged kaons, protons and antiprotons, (excluding products of K^0_S, Λ, and $\bar{\Lambda}$ decays) in the same region of $P_{\mathrm{T}}^{\mathrm{LAB}}$ and η^{LAB} as the K^0_S.

In Figs. 18 and 19, $\mathcal{T}$ is shown as a function of $P_{\mathrm{T}}^{\mathrm{LAB}}$ and η^{LAB} for the high-Q^2 sample (for the low-Q^2 sample, not shown, the values are similar) and for the photoproduction sample. The MC predictions from ARIADNE and PYTHIA are also shown. They follow the data reasonably well, preferring the strangeness-suppression factor to be smaller than 0.3. The measured $\mathcal{T}$ lies between 0.05 and 0.1, varying with $P_{\mathrm{T}}^{\mathrm{LAB}}$ for both the DIS and photoproduction. Similar values have been measured at e^+e^- [70] for the ratio of the number of K^0_S to the number of charged pions and are on average about 0.07 at centre-of-mass energies from 10 to 35 GeV, about 0.06 at the Z^0 and about 0.05 at 200 GeV. It can be concluded that $\mathcal{T}$ is about the same in e^+e^- and ep.

In order to see whether $\mathcal{T}$ depends on the transverse energy flow, the fireball selection, as discussed above, was applied to the photoproduction events. Figure 19c and d show the measured and predicted $\mathcal{T}$ for the fireball selection. The quantity $\mathcal{T}$ hardly depends on the fireball selection, as predicted by PYTHIA.

Fireball events are candidates for events where QCD instantons [33–43] could play a role [102–104], since they are characterised by isotropic transverse energy flow. Another expectation is a likely enhancement of heavier-quark

production relative to light quarks, due to the required flavour democracy. Searches for QCD instantons in DIS have been reported by H1 [105] and ZEUS [106]. No effect was identified due to QCD instantons, as the expected effects were small compared to the background at the relatively large Q^2 required. Bigger effects are expected at lower Q^2.

If QCD instantons contribute to the fireball event sample, then $\mathcal{T}$ would be expected to be different, possibly larger, for the fireball events than the typical value of about 0.07 or 0.08. As this is not the case, this measurement of $\mathcal{T}$ in photoproduction does not support the idea that QCD instantons contribute significantly to the production of the fireball events. It should be noted that there is only a qualitative prediction on the contribution from QCD instantons based on democracy of flavours, including heavy flavours, subject to available energy. The only existing calculation [104] applies to DIS and only considers three massless flavours. Since there is no charm-quark contribution, this calculation is probably only valid at low particle multiplicities, where the number of K^0_S is predicted to be about twice as big as that predicted by ARIADNE.

6.5 Polarization

In analogy with QED, the spin-orbit interaction leads to polarization in scattering due to the strong inter-

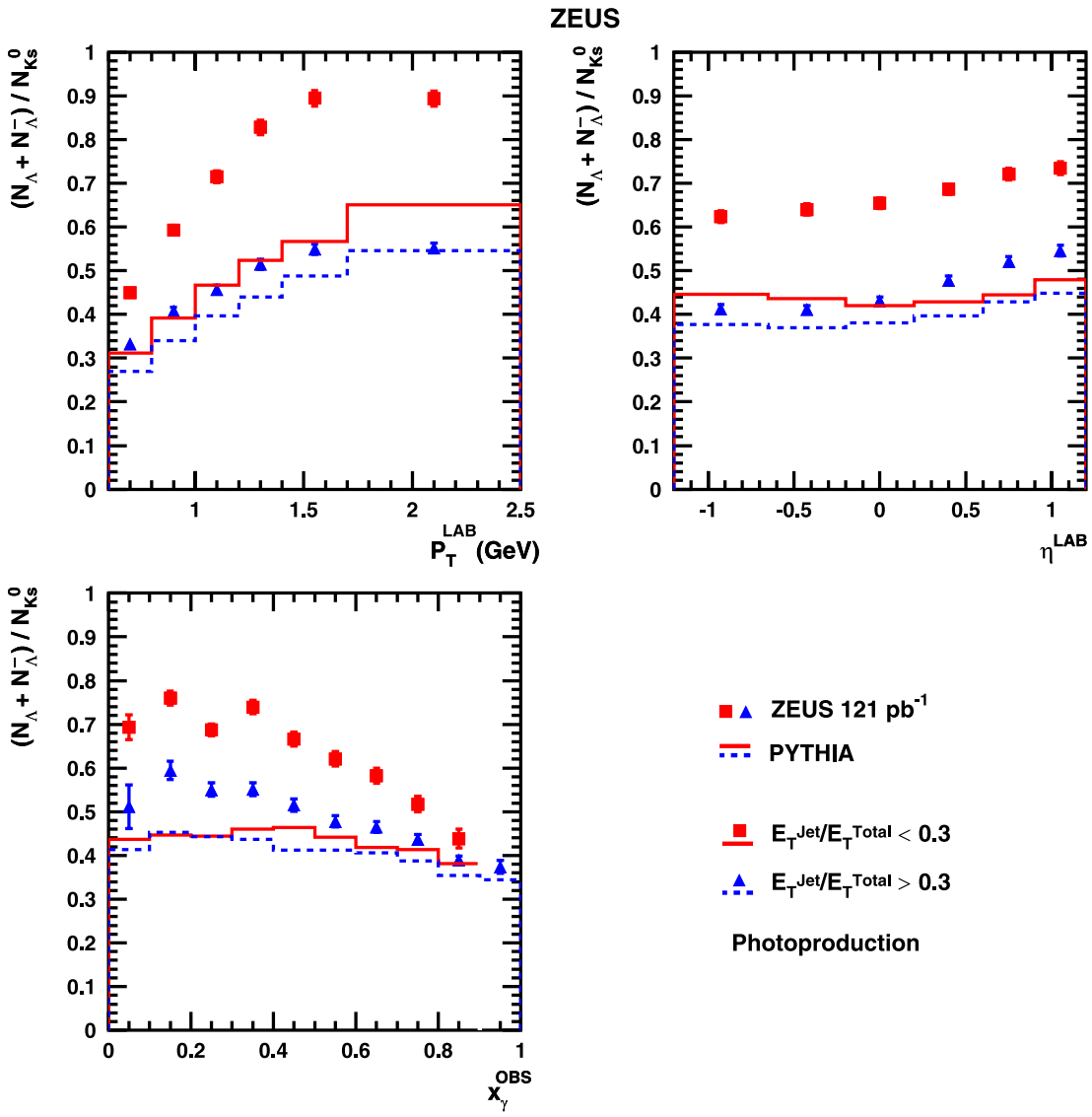

Fig. 17. The ratio $\frac{N(\Lambda)+N(\bar{\Lambda})}{N(K^0_S)}$ as a function of $P_{\rm T}^{\rm LAB}$, $\eta^{\rm LAB}$ and $x_\gamma^{\rm OBS}$, in the range $0.6 < P_{\rm T}^{\rm LAB} < 2.5$ GeV and $|\eta^{\rm LAB}| < 1.2$ for events with $Q^2 < 1\,{\rm GeV}^2$, $0.2 < y < 0.85$ and at least two jets both satisfying $E_{\rm T}^{\rm jet} > 5$ GeV and $|\eta^{\rm jet}| < 2.4$. The ratios from the fireball-enriched sample (*squares*) and the fireball-depleted sample (*triangles*) are shown for the data. The prediction from PYTHIA for the fireball-enriched (*solid line*) and for the fireball-depleted (*dashed line*) samples are shown. Statistical errors are shown. The highest $x_\gamma^{\rm OBS}$ bin ($0.9 < x_\gamma^{\rm OBS} < 1.0$) of the fireball enriched sample is omitted due to insufficient statistics

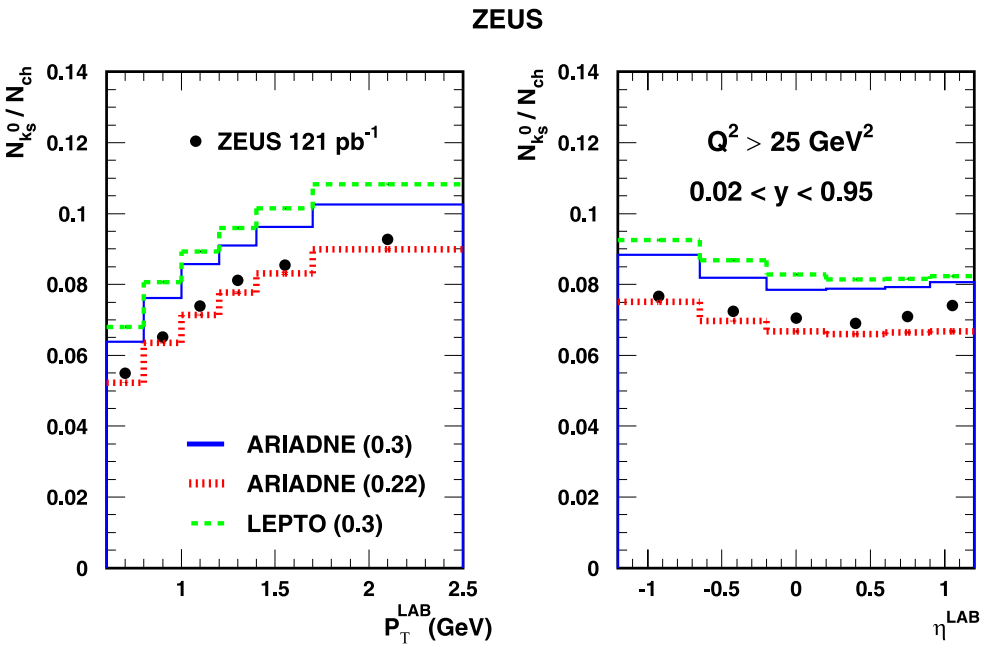

Fig. 18. The ratio $\frac{N(K^0_S)}{N_{ch}}$ as a function of P_T^{LAB} and η^{LAB}, in the range $0.6 < P_T^{LAB} < 2.5$ GeV and $|\eta^{LAB}| < 1.2$ for events with $Q^2 > 25\,\mathrm{GeV}^2$ and $0.02 < y < 0.95$. Statistical errors are smaller than the point size. The histograms show predictions from ARIADNE and LEPTO using the stated strangeness suppression

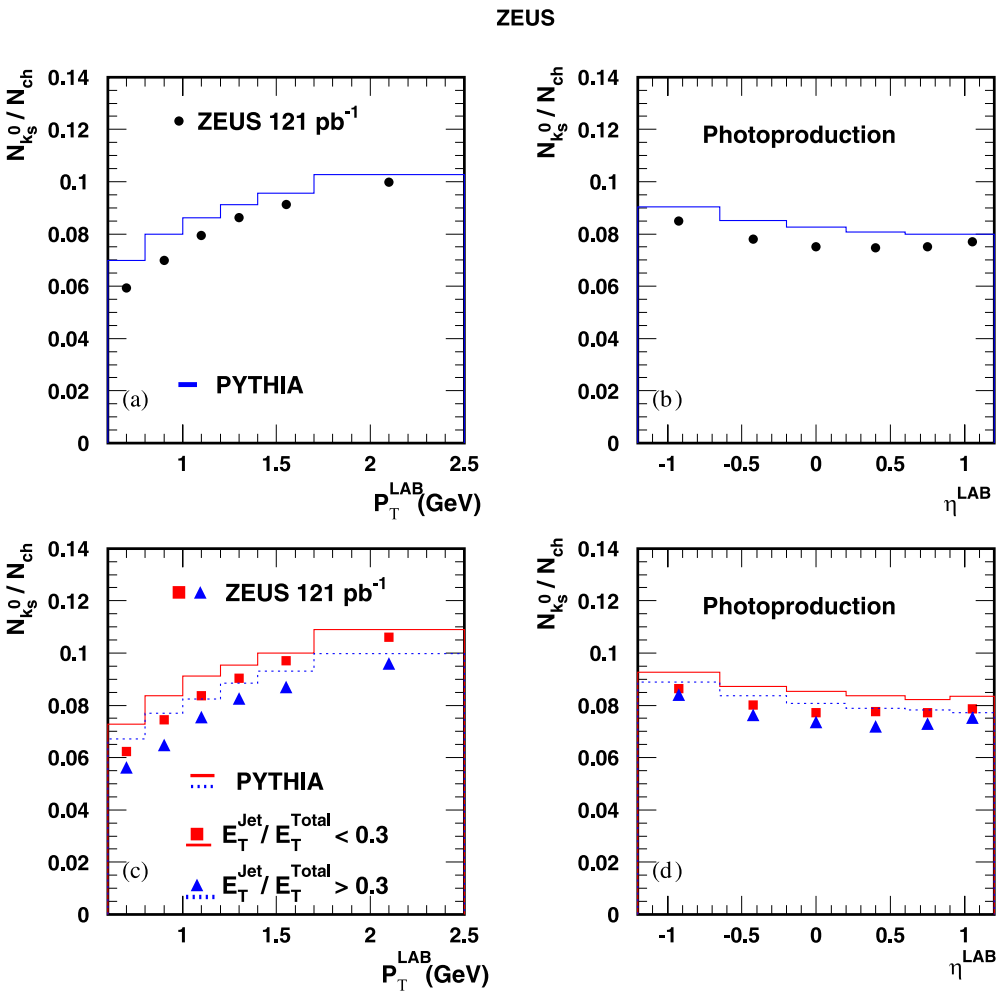

Fig. 19. The ratio $\frac{N(K^0_S)}{N_{ch}}$ as a function of P_T^{LAB} and η^{LAB}, in the range $0.6 < P_T^{LAB} < 2.5$ GeV and $|\eta^{LAB}| < 1.2$ for events with $Q^2 < 1\,\mathrm{GeV}^2$, $0.2 < y < 0.85$ and at least two jets both satisfying $E_T^{jet} > 5$ GeV and $|\eta^{jet}| < 2.4$. The ratio is shown for all events in **a** and **b** and for the fireball-enriched sample and the fireball-depleted sample in **c** and **d**. Prediction from PYTHIA (with multiple interactions) predictions with a strangeness suppression factor of 0.3 are shown as *solid* and *dashed histograms*. Statistical errors are smaller than the *symbols*

action [44–46]. Unpolarized s quarks get partially transversely polarized due to elastic scattering in the coloured field along the direction of $\mathbf{k}_i \times \mathbf{k}_f$, where $\mathbf{k}_i$ and $\mathbf{k}_f$ stand for the initial and final momenta of the s quarks. The degree of the polarization depends on the scattering angle and the strength of the coloured field. In the constituent quark

	Polarization (%)		
	High-Q^2 DIS	Low-Q^2 DIS	Photoproduction
Λ	$-1.3 \pm 4.3(\text{stat.})^{+4.0}_{-0.8}(\text{syst.})$	$-4.0 \pm 5.3(\text{stat.})^{+4.7}_{-4.0}(\text{syst.})$	$-2.4 \pm 2.2(\text{stat.})$
$\bar{\Lambda}$	$-2.2 \pm 4.2(\text{stat.})^{+2.4}_{-1.3}(\text{syst.})$	$-8.5 \pm 5.5(\text{stat.})^{+4.7}_{-2.1}(\text{syst.})$	$-5.8 \pm 2.2(\text{stat.})$
K^0_S	$-1.5 \pm 1.1(\text{stat.})$	$-0.05 \pm 1.5(\text{stat.})$	$-0.5 \pm 0.2(\text{stat.})$

Table 1. The transverse polarization values for Λ and $\bar{\Lambda}$, expressed here in %, in the high-Q^2 DIS ($Q^2 > 25\,\text{GeV}^2$ and $0.02 < y < 0.95$), low-Q^2 DIS ($5 < Q^2 < 25\,\text{GeV}^2$ and $0.02 < y < 0.95$), and photoproduction ($Q^2 < 1\,\text{GeV}^2$, $0.2 < y < 0.85$ and with two jets $E_{\text{T}}^{\text{jet}} > 5\,\text{GeV}$ and $|\eta^{\text{jet}}| < 2.4$) samples. Only Λ and $\bar{\Lambda}$ in the range $0.6 < P_{\text{T}}^{\text{LAB}} < 2.5\,\text{GeV}$ and $|\eta^{\text{LAB}}| < 1.2$ are considered. The statistical error is quoted for all samples, together with the systematic uncertainty associated with the measurement for the high-Q^2 and low-Q^2 samples. A similar systematic uncertainty is expected for the photoproduction sample. Also shown, as a test of any systematic effect, are the polarization values obtained by investigating the angular distribution of the higher-momentum π from K^0_S decays

model, the Λ inherits its spin from the s quark, and $\mathbf{k}_{\text{f}}$ is along the Λ momentum. As $\mathbf{k}_i$ is unknown in our case, the electron beam direction was used instead (the effect of using the jet direction was also investigated).

The transverse polarization $\mathcal{P}^{\Lambda}$ ($\mathcal{P}^{\bar{\Lambda}}$) is defined by the form of the proton (antiproton) angular distribution:

$$\frac{1}{N}\frac{\mathrm{d}N}{\mathrm{d}\cos\theta} = \frac{1}{2}[1 + \alpha\mathcal{P}^{\Lambda}\cos\theta]\,,$$
$$\frac{1}{N}\frac{\mathrm{d}N}{\mathrm{d}\cos\theta} = \frac{1}{2}[1 - \alpha\mathcal{P}^{\bar{\Lambda}}\cos\theta]\,,$$

where α is the decay asymmetry parameter, measured to be $\alpha = 0.642 \pm 0.013$ [70], and θ is the angle between the proton (antiproton) momentum boosted to the rest frame of the $\Lambda(\bar{\Lambda})$ and the polarization axis, $k_{\text{e}}^{\text{beam}} \times k_{\Lambda}$. An example of the angular distribution of the proton's (antiproton's) momenta with respect to the polarization axis, boosted to the $\Lambda(\bar{\Lambda})$ rest frame, is shown in Fig. 20.

Fitted values of the transverse polarization $\mathcal{P}^{\Lambda}$ and $\mathcal{P}^{\bar{\Lambda}}$ are presented in Table 1 for high- and low-Q^2 DIS and for photoproduction. All values are compatible with no polarization. Also presented are the polarization values obtained by investigating the angular distribution of the higher-momentum π from K^0_S decays, as a further test of any systematic detector effect.

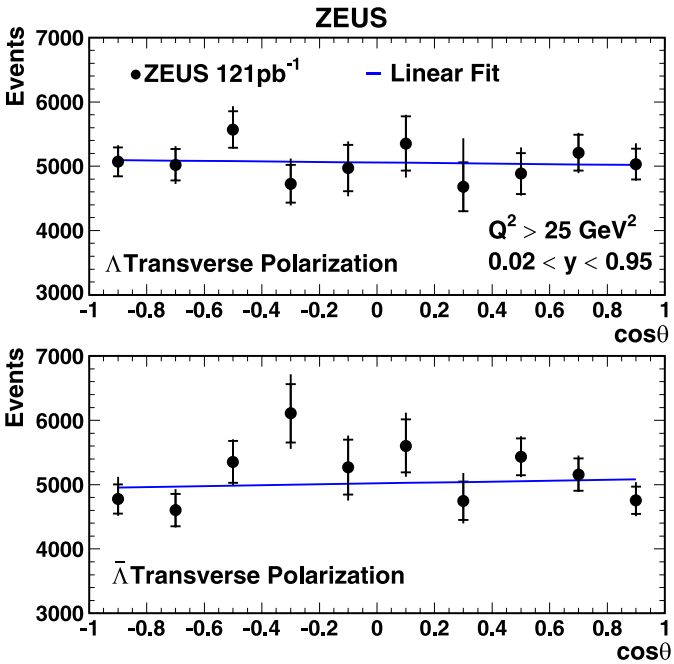

Fig. 20. Angular distributions of the highest-momentum decay particle from a Λ or $\bar{\Lambda}$ in the range $0.6 < P_{\text{T}}^{\text{LAB}} < 2.5\,\text{GeV}$ and $|\eta^{\text{LAB}}| < 1.2$ for events with $Q^2 > 25\,\text{GeV}^2$ and $0.02 < y < 0.95$, where θ is the angle between the decay-particle momentum vector and the polarization axis, in the rest frame of the Λ or $\bar{\Lambda}$. Statistical errors (inner error bars) and the systematic uncertainties added in quadrature are shown. The first-order polynomial fit (*solid line*) from which the polarization is obtained is also shown

7 Conclusions

Measurements of K^0_S, Λ and $\bar{\Lambda}$ production have been made at HERA, using $121\,\text{pb}^{-1}$ of data collected with the ZEUS detector. The following conclusions have been obtained:

1. in high- and low-Q^2 DIS, ARIADNE reproduces gross features of the cross sections but shows discrepancies in detail. Overall, the strangeness suppression factor $\lambda_s = 0.3$ is preferred to $\lambda_s = 0.22$. PYTHIA, normalised to the data, describes the dependence of the photoproduction cross sections on $P_{\text{T}}^{\text{LAB}}$ and η^{LAB} satisfactorily but fails to reproduce the x_{γ}^{OBS} dependence;
2. the numbers of Λ and $\bar{\Lambda}$ produced are consistent with being equal;
3. except for the resolved photon interactions, the measured ratio of baryons to mesons $\mathcal{R}$, defined as:

$$\mathcal{R} = \frac{N(\Lambda) + N(\bar{\Lambda})}{N(K^0_S)}\,,$$

is in the range between 0.2 and 0.5, similar to measurements at e^+e^- colliders. ARIADNE and PYTHIA

follow the shapes of the data on the selected observables but in many cases fail quantitatively at the 10 to 20% level;
4. in the resolved photon region, the ratio of baryons to mesons is large, significantly larger than measured in e^+e^- interactions and significantly larger than the PYTHIA prediction;
5. the ratio of strange-to-light hadrons measured in terms of $\mathcal{T}$:

$$\mathcal{T} = \frac{N(K^0_S)}{N_{\rm ch}},$$

is compatible with measurements at other colliders and is described by ARIADNE and PYTHIA for all investigated samples of events. For the DIS sample, the strangeness suppression factor $\lambda_s = 0.22$ is preferred to the default value of $\lambda_s = 0.3$. For the photoproduction sample, PYTHIA with $\lambda_s = 0.3$ overestimates the data, but describes the shape of the distributions. There is no indication of any unusual yield of strange-hadrons in the fireball-enriched sample, as would be qualitatively expected had there been a significant contribution from QCD instantons;
6. No evidence has been found for non-zero transverse polarization in inclusive Λ or $\bar{\Lambda}$ production.

Acknowledgements. We thank the DESY directorate for its strong support and encouragement. The remarkable achievements of the HERA machine group were essential for the successful completion of this work and are greatly appreciated. The design, construction and installation of the ZEUS detector have been made possible by the efforts of many people who are not listed as authors.

References

1. TASSO Collaboration, M. Althoff et al., Z. Phys. C **27**, 27 (1985)
2. TASSO Collaboration, W. Braunschweig et al., Z. Phys. C **47**, 167 (1990)
3. TPC Collaboration, H. Aihara et al., Phys. Rev. Lett. **54**, 274 (1985)
4. MARK-II Collaboration, C. De La Vaissiere et al., Phys. Rev. Lett. **54**, 2071 (1985)
5. MARK-II Collaboration, H. Schellman et al., Phys. Rev. D **31**, 3013 (1985)
6. HRS Collaboration, M. Derrick et al., Phys. Rev. D **35**, 2639 (1987)
7. TASSO Collaboration, R. Brandelik et al., Phys. Lett. B **105**, 75 (1981)
8. TASSO Collaboration, W. Braunschweig et al., Z. Phys. C **45**, 209 (1989)
9. CELLO Collaboration, H. Behrend et al., Z. Phys. C **46**, 397 (1990)
10. ALEPH Collaboration, D. Buskulic et al., Z. Phys. C **64**, 361 (1994)
11. DELPHI Collaboration, P. Abreu et al., Phys. Lett. B **318**, 249 (1993)
12. DELPHI Collaboration, P. Abreu et al., Z. Phys. C **65**, 587 (1995)
13. L3 Collaboration, M. Acciarri et al., Phys. Lett. B **328**, 223 (1994)
14. OPAL Collaboration, P. Acton et al., Phys. Lett. B **291**, 503 (1992)
15. OPAL Collaboration, R. Akers et al., Z. Phys. C **67**, 389 (1995)
16. ZEUS Collaboration, M. Derrick et al., Z. Phys. C **68**, 29 (1995)
17. ZEUS Collaboration, J. Breitweg et al., Eur. Phys. J. C **2**, 77 (1998)
18. H1 Collaboration, S. Aid et al., Nucl. Phys. B **480**, 3 (1996)
19. H1 Collaboration, C. Adloff et al., Z. Phys. C **76**, 213 (1997)
20. UA5 Collaboration, R. Ansorge et al., Z. Phys. C **41**, 179 (1988)
21. UA5 Collaboration, R. Ansorge et al., Nucl. Phys. B **328**, 36 (1989)
22. CDF Collaboration, D. Acosta et al., Phys. Rev. D **72**, 052 001 (2005)
23. UA1 Collaboration, G. Bocquet et al., Phys. Lett. B **366**, 441 (1996)
24. STAR Collaboration, B.I. Abelev et al., Preprint nucl-ex/0607033 (2006)
25. L. Lönnblad, Comput. Phys. Commun. **71**, 15 (1992)
26. G. Ingelman, A. Edin, J. Rathsman, Comput. Phys. Commun. **101**, 108 (1997)
27. H. Jung, Comput. Phys. Commun. **86**, 147 (1995)
28. T. Sjöstrand et al., Comput. Phys. Commun. **135**, 238 (2001)
29. G. Corcella et al., Preprint hep-ph/0210213, 2002
30. B. Kopeliovich, B. Povh, Z. Phys. C **75**, 693 (1997)
31. R. Fries et al., Phys. Rev. Lett. **90**, 202 303 (2003)
32. S. Bass, B. Müller, D. Srivastava, Phys. Rev. Lett. **91**, 052 302 (2003)
33. A. Belavin et al., Phys. Lett. B **59**, 85 (1975)
34. G. 't Hooft, Phys. Rev. Lett. **37**, 8 (1976)
35. G. 't Hooft, Phys. Rev. D **14**, 3432 (1976)
36. G. 't Hooft, Phys. Rev. D **18**, 2199 (1978)
37. G. 't Hooft, Phys. Rep. **142**, 357 (1986)
38. H. Aoyama, H. Goldberg, Phys. Lett. B **188**, 506 (1987)
39. A. Ringwald, Nucl. Phys. B **330**, 1 (1990)
40. O. Espinosa, Nucl. Phys. B **343**, 310 (1990)
41. A. Ringwald et al., Nucl. Phys. B **365**, 3 (1991)
42. M. Gibbs et al., Z. Phys. C **66**, 285 (1995)
43. A. Ringwald, Phys. Lett. B **555**, 227 (2002)
44. J. Szwed, Phys. Lett. B **105**, 403 (1981)
45. A. Panagiotou, Int. J. Mod. Phys. A **5**, 1197 (1989)
46. J. Gago, R. Vilela Mendes, P. Vaz, Phys. Lett. B **183**, 357 (1987)
47. ZEUS Collaboration, U. Holm (Ed.), The ZEUS Detector, Status Report (unpublished), DESY (1993), available on http://www-zeus.desy.de/bluebook/bluebook.html
48. N. Harnew et al., Nucl. Instrum. Methods A **279**, 290 (1989)
49. B. Foster et al., Nucl. Phys. B Proc. Suppl. **32**, 181 (1993)
50. B. Foster et al., Nucl. Instrum. Methods A **338**, 254 (1994)
51. M. Derrick et al., Nucl. Instrum. Methods A **309**, 77 (1991)
52. A. Andresen et al., Nucl. Instrum. Methods A **309**, 101 (1991)
53. A. Caldwell et al., Nucl. Instrum. Methods A **321**, 356 (1992)
54. A. Bernstein et al., Nucl. Instrum. Methods A **336**, 23 (1993)

55. ZEUS Collaboration, J. Breitweg et al., Eur. Phys. J. C **1**, 109 (1998)
56. J. Andruszków et al., Preprint [DESY-92-066], DESY (1992)
57. ZEUS Collaboration, M. Derrick et al., Z. Phys. C **63**, 391 (1994)
58. J. Andruszków et al., Acta Phys. Pol. B **32**, 2025 (2001)
59. H. Abramowicz, A. Caldwell, R. Sinkus, Nucl. Instrum. Methods A **365**, 508 (1995)
60. R. Sinkus, T. Voss, Nucl. Instrum. Methods A **391**, 360 (1997)
61. J.D. Bjorken, E.A. Paschos, Phys. Rev. **185**, 1975 (1969)
62. S. Bentvelsen, J. Engelen, P. Kooijman, Proc. Workshop on Physics at HERA, ed. by W. Buchmüller, G. Ingelman (Hamburg, Germany, DESY, 1992) Vol. 1, p. 23
63. K.C. Höger, Proc. Workshop on Physics at HERA, ed. by W. Buchmüller, G. Ingelman (Hamburg, Germany, DESY, 1992) Vol. 1, p. 43
64. F. Jacquet, A. Blondel, Proc. of the Study for an *ep* Facility for Europe, ed. by U. Amaldi (Hamburg, Germany, 1979) p. 391, Also in preprint DESY 79/48
65. S. Catani et al., Phys. Lett. B **285**, 291 (1992)
66. S. Catani et al., Nucl. Phys. B **406**, 187 (1993)
67. S.D. Ellis, D.E. Soper, Phys. Rev. D **48**, 3160 (1993)
68. ZEUS Collaboration, J. Breitweg et al., Eur. Phys. J. C **11**, 35 (1999)
69. P. Billoir, S. Qian, Nucl. Instrum. Methods A **311** (1992)
70. Particle Data Group, S. Eidelman et al., Phys. Lett. B **592**, 1 (2004)
71. R. Brun et al., GEANT3, Technical Report CERN-DD/EE/84-1, CERN (1987)
72. A. Kwiatkowski, H. Spiesberger, H.-J. Möhring, Comput. Phys. Commun. **69**, 155 (1992)
73. K. Charchula, G.A. Schuler, H. Spiesberger, Comput. Phys. Commun. **81**, 381 (1994)
74. H. Spiesberger, An Event Generator for *ep* Interactions at HERA Including Radiative Processes (Version 4.6) (1996) available on http://www.desy.de/ ∼hspiesb/heracles.html
75. H. Spiesberger, HERACLES and DJANGOH: Event Generation for *ep* Interactions at HERA Including Radiative Processes (1998), available on http://www.desy.de/∼hspiesb/djangoh.html
76. H.L. Lai et al., Phys. Rev. D **55**, 1280 (1997)
77. CTEQ Collaboration, H.L. Lai et al., Eur. Phys. J. C **12**, 375 (2000)
78. B. Andersson et al., Phys. Rep. **97**, 31 (1983)
79. OPAL Collaboration, P.D. Acton et al., Z. Phys. C **56**, 521 (1992)
80. OPAL Collaboration, R. Akers et al., Z. Phys. C **68**, 1 (1995)
81. ALEPH Collaboration, D. Buskulic et al., Z. Phys. C **69**, 379 (1996)
82. DELPHI Collaboration, P. Abreu et al., Z. Phys. C **73**, 61 (1996)
83. T. Sjöstrand, L. Lönnblad, S. Mrenna, Preprint hep-ph/0108264 (2001)
84. E665 Collaboration, M. Adams et al., Z. Phys. C **61**, 539 (1994)
85. SLD Collaboration, K. Abe et al., Phys. Rev. D **59**, 052 001 (1999)
86. ZEUS Collaboration, S. Chekanov et al., Phys. Lett. B **553**, 141 (2002)
87. M. Glück, E. Reya, A. Vogt, Z. Phys. C **67**, 433 (1995)
88. G.A. Schuler, T. Sjöstrand, Z. Phys. C **68**, 607 (1995)
89. T. Sjöstrand, M. van Zijl, Phys. Rev. D **36**, 2019 (1987)
90. G. Schuler, T. Sjöstrand, Phys. Lett. B **300**, 169 (1993)
91. G. Schuler, T. Sjöstrand, Nucl. Phys. B **407**, 539 (1993)
92. J. Butterworth, J. Forshaw, J. Phys. G **19**, 1657 (1993)
93. H1 Collaboration, S. Aid et al., Z. Phys. C **70**, 17 (1996)
94. ZEUS Collaboration, S. Chekanov et al., Eur. Phys. J. C **44**, 351 (2005)
95. PHENIX Collaboration, K. Adcox et al., Phys. Rev. Lett. **89**, 092 302 (2002)
96. D.A. Mason, Phd thesis, FERMILAB-THESIS-2006-01
97. STAR Collaboration, J. Adams et al., Phys. Lett. B **637**, 161 (2006)
98. PHENIX Collaboration, S. Adler et al., Phys. Rev. C **69**, 034 909 (2004)
99. STAR Collaboration, C. Adler et al., Phys. Rev. Lett. **89**, 092 301 (2002)
100. STAR Collaboration, J. Adams et al., Phys. Rev. Lett. **92**, 112 301 (2004)
101. STAR Collaboration, J. Adams et al., Phys. Lett. B **595**, 143 (2004)
102. A. Ringwald, F. Schrempp, Preprint hep-ph/9411217 (1994)
103. C. Nath, R. Walczak, Y. Yamazaki, J. Phys. G **25**, 1440 (1999)
104. T. Carli et al., Preprint hep-ph/9906441 (1999)
105. H1 Collaboration, C. Adloff et al., Eur. Phys. J. C **25**, 495 (2002)
106. ZEUS Collaboration, S. Chekanov et al., Eur. Phys. J. C **34**, 255 (2004)